Discovery of 4-{4-[3-(Pyridin-2-yl)-1*H*-pyrazol-4-yl]pyridin-2-yl}-*N*-(tetrahydro-2*H*-pyran-4-yl)benzamide (GW788388): A Potent, Selective, and Orally Active Transforming Growth Factor-β Type I Receptor Inhibitor

Françoise Gellibert,*,† Anne-Charlotte de Gouville,‡ James Woolven,§ Neil Mathews,⊗,|| Van-Loc Nguyen,† Cécile Bertho-Ruault,† Angela Patikis,⊥ Eugene T. Grygielko,▽ Nicholas J. Laping,▽ and Stéphane Huet‡

Department of Medicinal Chemistry and Biology, GlaxoSmithKline, 25−27 Avenue du Québec, 91951 Les Ulis, France, Computational and Structural Sciences, Department of Drug Metabolism and Pharmacokinetics, GlaxoSmithKline, GunnelsWood Road, Stevenage, Hertfordshire SG1 2NY, United Kingdom, Department of Medicinal Chemistry, GlaxoSmithKline, Gunnels Wood Road, Stevenage, Hertfordshire SG1 2NY, United Kingdom, and Departments of Renal and Urology Research, GlaxoSmithKline Pharmaceuticals, King of Prussia, Pennsylvania

Received October 5, 2005

Inhibitors of transforming growth factor β (TGF-β) type I receptor (ALK5) offer a novel approach for the treatment of fibrotic diseases such as renal, hepatic, and pulmonary fibrosis. The optimization of a novel phenylpyridine pyrazole series (**1a**) led to the identification of potent, selective, and orally active ALK5 inhibitors. The cellular potency and pharmacokinetics profiles of these derivatives were improved and several compounds presented antifibrotic activity when orally administered to rats in an acute liver model of dimethylnitrosamine- (DMN-) induced expression of collagen IA1 mRNA, a major gene contributing to excessive extra cellular matrix deposit. One of the most potent ALK5 inhibitors identified in this chemical series, compound **13d** (GW788388), reduced the expression of collagen IA1 by 80% at a dose of 1 mg/kg twice a day (b.i.d.). This compound significantly reduced the expression of collagen IA1 mRNA when administered orally at 10 mg/kg once a day (u.i.d.) in a model of puromycin aminonucleoside-induced renal fibrosis.

Introduction

Transforming growth factor β1 (TGF-β1) is the prototypic member of a superfamily of ligands involved in the regulation of numerous developmental and physiological processes but also in pathological processes such as cancer and fibrosis. While TGF-β has both a tumor suppressor and tumor promoter role depending on the tumor type and stage of metastasis, its role in fibrosis is well established. TGF-β1 is a pluripotent cytokine that not only regulates the extracellular matrix (ECM) deposition in response to tissue injury, thus contributing to the healing process, but also is involved in pathological fibrosis including pulmonary fibrosis, liver fibrosis, and renal glomerulosclerosis.[1] Therefore, inhibition of TGF-β signaling is thought to be a viable approach to treat fibrosis. Members of the TGF-β superfamily, such as TGF-β1, TGF-β2, and TGF-β3, activins, inhibins, bone morphogenetic proteins, and Müllerian-inhibiting substance, signal through a family of transmembrane serine/threonine kinase receptors. These receptors can be divided into two classes, the type I or activin-like kinase (ALK) receptors and type II receptors. Specifically, the binding of TGF-β1 to the type II receptor causes phosphorylation of the GS domain of the TGF-β type I receptor, ALK5. The ALK5 receptor, in turn, phosphorylates the cytoplasmic proteins smad2 and smad3 at two carboxy-terminal serines. The phosphorylated smad proteins form heteromeric complexes of smad2, smad3, and smad4, after which the complex translocates into the nucleus to affect gene transcription.[2]

Several approaches have been used to interfere with the TGF-β pathway in liver and renal models of fibrosis. Indeed compared to wild-type animals, smad3 heterozygous or homozygous knockout animals do not show as much a reduced increase in liver matrix gene expression following acute administration of CCl_4, a liver-damaging agent.[3] Similarly, a truncated recombinant TGF-β type II receptor that specifically inhibits TGF-β signaling as a dominant negative receptor has been described to show antifibrotic effects in a liver fibrosis model.[4] Transgenic mice that overexpress TGF-β1 develop severe glomerulosclerosis,[5] and neutralizing antibodies against TGF-β1 can prevent the accumulation of extracellular matrix in diabetic models of renal disease, translating into an improved renal function.[6] Therapeutic approaches based on gene therapy or injection of recombinant proteins have limitations, and a selective targeting of the TGF-β signaling pathway by use of direct inhibitors of ALK5 represents an attractive alternative to prevent detrimental profibrotic effects of TGF-β.

Recently we reported the identification and optimization of an aminothiazole quinoline series **I** that led to potent and selective ALK5 inhibitors **II** and **III** (Chart 1).[7] We demonstrated, from X-ray crystallographic data, that the binding mode for the naphthyridine pyrazole compound **III** (R═CH_3) was comparable to that described by Sawyer et al.[8] for other families of pyrazoles **IV** and **V** (Chart 2). From the quinoline compound **I** we designed other chemical series. The main structural modifications were to replace both the central core and the quinoline moiety with different heterocycles while maintaining the nitrogen atoms that were involved in major hydrogen-bond interactions with the binding site. This approach led to the

* To whom correspondence should be addressed: tel +33 1 69 29 61 28; fax +33 1 69 07 48 92; e.mail francoise.gellibert@gsk.com.
† Department of Medicinal Chemistry, GlaxoSmithKline, Les Ulis.
‡ Department of Biology, GlaxoSmithKline, Les Ulis.
§ Computational and Structural Sciences, GlaxoSmithKline, Stevenage.
⊗ Department of Medicinal Chemistry, GlaxoSmithKline, Stevenage.
|| Present address: Arrow Therapeutics, Britannia House, 7 Trinity St., London SE1 1DA, U.K.
⊥ Department of Drug Metabolism and Pharmacokinetics, GlaxoSmithKline, Stevenage.
▽ Departments of Renal and Urology Research, GlaxoSmithKline.

10.1021/jm0509905 CCC: $33.50 © 2006 American Chemical Society
Published on Web 03/16/2006

Chart 1

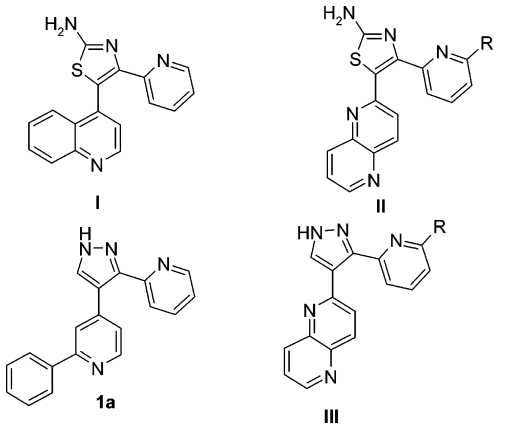

Chart 2

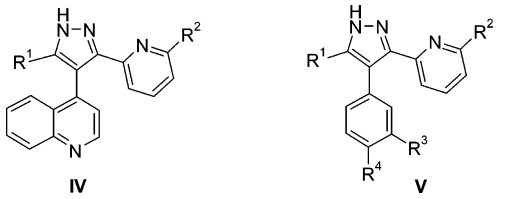

identification of the phenylpyridine pyrazole **1a** that exhibited ALK5 binding affinity (IC_{50} = 107 nM) and a moderate cellular activity (IC_{50} = 519 nM) when evaluated in a TGF-β-dependent transcriptional assay with HepG2 cells stably transfected with the TGF-β responsive PAI-1 promoter driving a luciferase reporter. Interestingly, **1a** presented in vivo activity in an acute model of dimethylnitrosamine- (DMN-) induced liver disease when administered orally at doses of 25 mg/kg b.i.d. and above.[9] This first result was very encouraging, and our efforts focused on the optimization of this new phenylpyridine pyrazole series. The present report describes the main modifications that improved both in vitro potency and pharmacokinetics parameters to enhance in vivo activity.

Chemistry

Two approaches were developed to synthesize these novel 2-phenyl-4-[3-(pyridin-2-yl)-1*H*-pyrazol-4-yl]pyridine derivatives. The first approach was based upon the construction of the pyrazole core at the end of the synthesis (Scheme 1). Commercially available 2-bromo-4-methylpyridine was coupled with substituted phenylboronic acids under palladium-catalyzed Suzuki standard conditions [$Pd(PPh_3)_4$, $NaHCO_3$, toluene, reflux] to afford the 2-phenyl-4-methylpyridine derivatives **2a**−**m**. Condensation with ethyl 2-pyridinecarboxylate in the presence of potassium bis(trimethylsilyl)amide at −50 °C gave the corresponding ketones **3a**−**m**. Therefore, reaction of **3a**−**m** with dimethylformamide dimethyl acetal (DMF·DMA) led to the nonisolated enamine intermediates, which were cyclized directly to pyrazoles **1a**−**m** by reaction with hydrazine monohydrate in DMF at room temperature.

The second approach was based upon the palladium-catalyzed Suzuki cross-coupling of a key pyrazole intermediate **6** with various arylboronic acids. In this case, the diversity of the commercially available boronic acids allowed us to explore different functions in the para position of the phenyl ring at the last step of the synthetic pathway. The pyrazole **5** was prepared in three steps (Scheme 2) as previously described in Scheme 1, and subsequent treatment with trityl chloride in the presence of potassium carbonate in acetone at room temperature gave the key intermediate **6**. Protection of the pyrazole was necessary to perform the subsequent coupling reactions; the trityl goup was chosen due to the possibility to further develop solid-phase synthesis from the corresponding resin. Compounds **1n,o** were obtained following this second approach (Scheme 2) by Suzuki coupling reaction with, respectively, the methyl carboxylate and cyanophenylboronic acids followed by the cleavage of the trityl group in acidic condition. From the corresponding boronic acids, different spacers were obtained: 4-hydroxy, 4-formyl, 4-carboxylate, or 4-amino (Scheme 3). Intermediate **7** was then coupled with halide derivatives in the presence of sodium hydride or potassium carbonate in acetone at room temperature to prepare the alkoxy compounds **11a**−**g**.

The methylamine derivatives **12a**−**c** were obtained by reductive amination of the benzaldehyde **8** with sodium triacetoxyborohydride in the presence of catalytic amount of acetic acid in dichloromethane.

The amido compounds **13a**−**e** were synthesized by coupling the acid **9** with amines in the presence of 1-hydroxybenzotriazole (HOBT) and 1-ethyl-3-(3-dimethylaminopropyl)carbodiimide (EDCI) at room temperature in dichloromethane. The inverse amide compound **14a** was obtained in an analogous manner

Scheme 1[a]

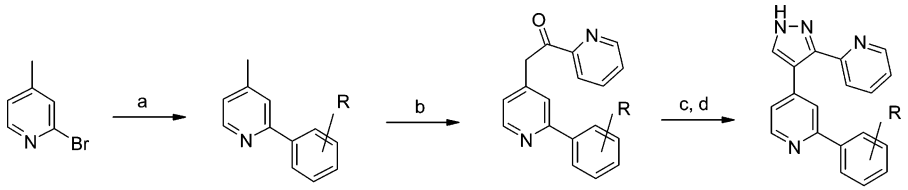

[a] Reagents and conditions: (a) Substituted phenylboronic acid, $Pd(PPh_3)_4$, Na_2CO_3, DME or toluene/EtOH, reflux; (b) ethyl 2-pyridinecarboxylate, KHMDS, THF, −50 °C; (c) DMF·DMA, DMF, room temperature; (d) hydrazine monohydrate, DMF, room temperature.

Scheme 2[a]

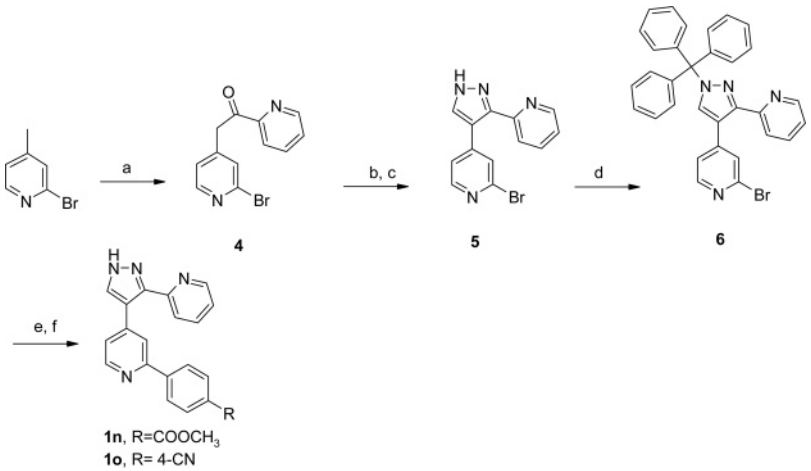

[a] Reagents and conditions: (a) Ethyl 2-pyridinecarboxylate, KHMDS, THF, −50 °C; (b) DMF·DMA, acetic acid, DMF, room temperature; (c) hydrazine monohydrate, DMF, room temperature; (d) trityl chloride, K_2CO_3, acetone, reflux, (e) 4-*R*-phenylboronic acid, $Pd(PPh_3)_4$, Na_2CO_3, DME or toluene/EtOH, reflux, (f) CF_3COOH, CH_2Cl_2, room temperature.

Scheme 3[a]

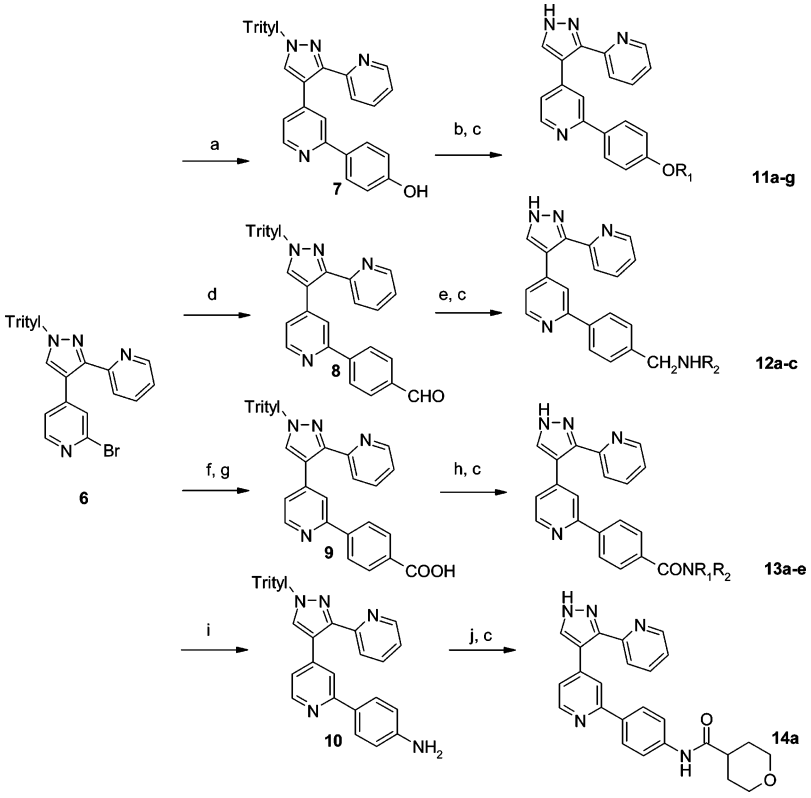

[a] Reagents and conditions: (a) 4-Hydroxyphenylboronic acid, $Pd(PPh_3)_4$, Na_2CO_3, DME or toluene/EtOH, reflux; (b) R^1X, NaH or K_2CO_3, DMF, room temperature; (c) MeOH/HCl 1 N; (d) 4-formylphenylboronic acid, $Pd(PPh_3)_4$, Na_2CO_3, DME, reflux; (e) R_2NH_2, AcOH, sodium triacetoxyborohydride, CH_2Cl_2, room temperature; (f) 4-(methoxycarbonylphenyl)boronic acid, $Pd(PPh_3)_4$, Na_2CO_3, toluene/EtOH, reflux; (g) 1 N NaOH, EtOH, reflux; (h) $R^1R^2NH_2$, HOBT, EDCI, CH_2Cl_2, room temperature (i) 4-aminophenylboronic acid, $Pd(PPh_3)_4$, Na_2CO_3, DME or toluene/EtOH, reflux; (j) tetrahydro-2*H*-pyran-4-carboxylic acid, HOBT, EDCI, CH_2Cl_2, room temperature.

starting from the amino **10**, with the last step for all these syntheses being the removal of the protecting group after treatment with 1 N HCl in methanol or with a mixture of trifluoroacetic acid/dichloromethane at 50 °C.

Results and Structure−Activity Relationship Discussion

All the compounds were tested in a fluorescence polarization (FP) binding assay,[15] in which the ability of test compounds to displace a rhodamine green-labeled ligand from recombinant glutathione S-transferase (GST)−ALK5 was measured. The most potent compounds were selected for evaluation in a TGF-β-dependent transcriptional assay.

At the outset of this work we had not yet obtained crystallographic data from a ligand cocrystallized with ALK5. From docking studies, based on the crystal structure of the ALK5−FKBP12 complex,[10] we established that **1a** was capable of binding in a manner similar to compounds **II** and **III**. This hypothesis was later strengthened by X-ray cocrystallization data.[7,8] Two main hydrogen-bond interactions are required to achieve binding potency: one between the nitrogen of the

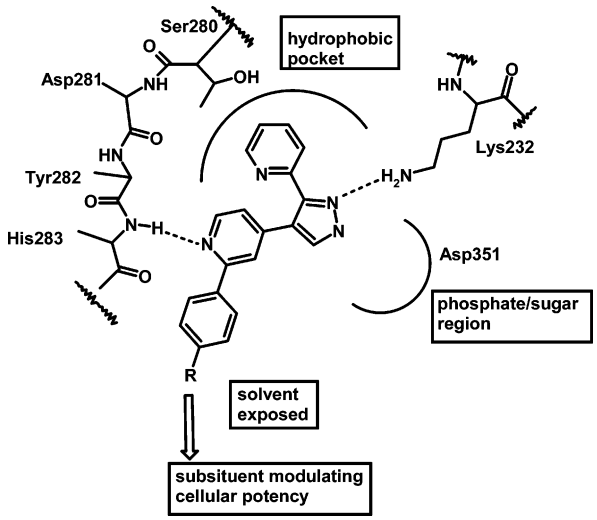

Figure 1. Schematic pharmacophore for (2-phenyl)pyridin-4-ylpyrazoles. Interactions between inhibitor and ALK5 residues are shown in dotted lines.

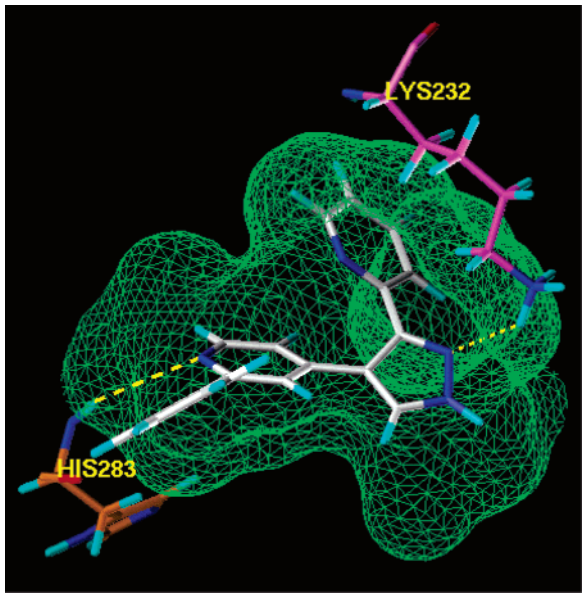

Figure 2. Connoly surface map of the modeling of **1a** into the ATP cleft of ALK5.

pyridin-4-yl group and the backbone NH of His-283, and a second between one of the two nitrogens of the pyrazole core and the side chain of Lys-232 (Figure 1). A third interaction could be envisaged between the second pyrazole nitrogen and Asp-351. The phenylpyridine moiety occupies a lipophilic pocket with a narrow cleft extending from the ubiquitous hydrogen bond (made between the pyridin-4-yl nitrogen and the backbone NH of His283) toward the outside of the protein (Figure 2). Therefore, it seemed attractive to focus the optimization of this new pyrazole series on the phenyl part of the molecule, which binds to a region of the ALK5 binding site of which we had little knowledge.

Initially, a limited range of substitution was carried out at the ortho, meta, and para positions of the phenyl ring to determine what were the tolerant positions for further exploration (Table 1). While the *o*-fluoro analogue **1b** was equipotent with **1a**, ortho substitution with larger groups such as methyl (**1c**) and trifluoromethyl (**1d**) gave a major decrease in binding affinity compared with the unsubstituted compound **1a**, while meta substitution (**1e**−**g**) retained similar binding potency to

Table 1. Substitution of the Phenyl Ring and Impact on Binding Affinity

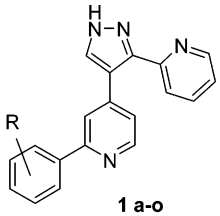

2-(Substituted phenyl)-4-[3-(pyridin-2-yl)-1H-pyrazol-4-yl]pyridine compounds

compd	R	IC_{50} for ALK5 binding[a] (μM)
1a	H	0.107 (0.028−0.415)
1b	2-F	0.059 (0.023−0.152)
1c	2-CH_3	3.981 (3.805−4.165)
1d	2-CF_3	9.333 (7.791−11.179)
1e	3-CH_3	0.191 (0.067−0.538)
1f	3-CF_3	0.240 (0.010−0.059)
1g	3-OCH_3	0.115 (0.080−0.165)
1h	4-CH_3	0.028 (0.010−0.076)
1i	4-CF_3	0.024 (0.024−0.024)
1j	4-OCH_3	0.024 (0.010−0.059)
1k	4-F	0.048 (0.033−0.069)
1l	4-^{i}Pr	0.032 (0.016−0.067)
1m	4-Cl	0.043 (0.041−0.045)
1n	4-COOMe	0.027 (0.019−0.039)
1o	4-CN	0.035 (0.029−0.042)

[a] Values are the mean of two or more separate experiments; pIC_{50}s were calculated, and mean pIC_{50} was converted to IC_{50}. Numbers in parentheses are the 95% confidence limits on the pIC_{50} converted to IC_{50} values and reported as the limits of the IC_{50}.

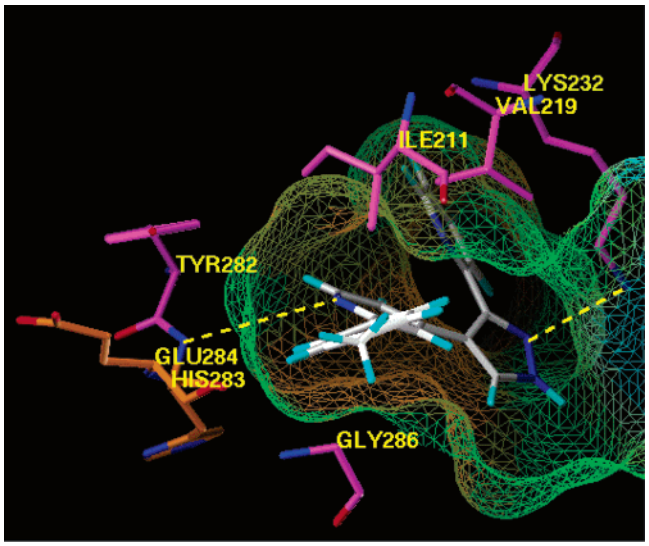

Figure 3. Connoly surface map of the modeling of **1h** into the ATP cleft of ALK5.

that of **1a**. On the other hand, introduction of para substituents such as methyl (**1h**), trifluoromethyl (**1i**), or methoxy (**1j**) increased potency compared with the unsubstituted compound (approximately 4-fold versus **1a**), and overall the effect of substitution position on ALK5-inhibitory potency followed the trend para > meta ≫ ortho. The generally lower binding affinity observed for substitution at the ortho and meta positions might be explained by steric constraints arising from interactions of the substituted aryl ring with the wall of the pocket in which it binds. Viewed from the open mouth of the active site as in Figure 3, the left side of the ligand phenyl group is closely bordered by the backbone of three adjacent residues, Tyr282, His283, and Glu284, and in particular Tyr282 projects its phenol

Table 2. Exploration of the Diversity at the 4-Position on the Phenyl Ring

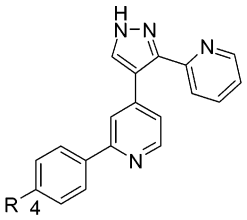

2-(4-substituted phenyl)-4-[3-(pyridin-2-yl)-1H-pyrazol-4-yl]pyridine compounds

compd	R	IC_{50} for ALK5 binding[a] (μM)	IC_{50} for TGF-β cellular assay[b] (μM)
1a	H	0.107 (0.028−0.415)	0.519 ± 0.061
1j	-OCH_3	0.024 (0.010−0.059)	0.537 ± 0.203
11a	-$O(CH_2)_2$-cyclohexyl	0.081 (0.032−0.210)	0.529 ± 0.467
11b	-$O(CH_2)_2Cl$	0.019 (0.019−0.019)	0.693 ± 0.358
11c	-OCH_2COCH_3	0.025 (0.018−0.036)	0.268 ± 0.124
11d	-$O(CH_2)_2N(CH_3)_2$	0.015 (0.002−0.151)	0.014 ± 0.005
11e	-$O(CH_2)_2$-pyrrolidine	0.040 (0.02−0.07)	0.050 ± 0.035
11f	-$O(CH_2)_2$-morpholine	0.012 (0.011−0.014)	0.209 ± 0.200
11g	-$O(CH_2)_2$-(imidazol-1-yl)	0.030 (0.021−0.110)	0.133 ± 0.106
12a	-CH_2-pyrrolidine	0.019 (0.016−0.022)	0.118 ± 0.054
12b	-CH_2-morpholine	0.042 (0.008−0.221)	0.358 ± 0.121
12c	-CH_2NH-(tetrahydro-2*H*-pyran-4-yl)	0.047 (0.020−0.110)	0.104 ± 0.024
13a	-$CONH(CH_2)_2OCH_3$	0.091 (0.064−0.131)	0.538 ± 0.318
13b	-CO-pyrrolidine	0.110 (0.08 to 0.14)	0.539 ± 0.098
13c	-CO-morpholine	0.123 (0.046−0.332)	0.257 ± 0.168
13d	-CO-[N-(tetrahydro-2*H*-pyran-4-ylamine)]	0.018 (0.003−0.094)	0.093 ± 0.045
13e	-CO-[*N*-methyl-(tetrahydro-2*H*-pyran-4-ylamine)]	0.214 (0.119−0.384)	1.691 ± 0.508
14a	-NHCO-(tetrahydro-2*H*-pyran-4-yl)	0.112 (0.071−0.176)	0.486 ± 0.192

[a] Values are the mean of two or more separate experiments; pIC_{50}s were calculated and mean pIC_{50} was converted to IC_{50}. Numbers in parentheses are the 95% confidence limits on the pIC_{50} converted to IC_{50} values and reported as the limits of the IC_{50}. [b] Mean values ± SD for a minimum of two determinations.

ring edge-on to the pocket containing the phenyl of the ligand. Above this region of the ligand lies Ile211, and above but further back, Val219 is close to one ortho position of the phenyl moiety. Below and similarly further back lies Leu340, while more directly below the phenyl of the ligand, the Cα of Gly286 is found.

Docking studies suggested that the *o*- and *m*-methyl compounds (**1c** and **1e**) might make less favorable interactions with the backbone amino acids (residues 282−284) that link the N- and C-terminal domains of the kinase (the hinge region) or unfavorable interactions with Ile211 (**1e**) or Val219 (**1c**) compared with the para analogue **1h** (Figure 3).

While para substitution appeared optimal for ALK5 inhibition, the nature of the substituent had no major impact on the binding potency;, indeed, a wide range of substituents was tolerated in this position (Table 1). From these first results we reasoned that modification of the substituent in this position might offer the potential to improve both the physicochemical properties and the cellular potency of this chemical series. Moreover, para substitution might also block metabolism and give an improved pharmacokinetic profile. Using the observation that the 4-methoxy analogue (**1j**) presented 4 times higher binding affinity than compound **1a** with comparable cellular activity, we decided first to investigate different side chains (neutral, polar, and basic) joined to the aryl ring via an ether link (Table 2). Encouragingly, the 2-cyclohexylethyl derivative **11a** showed a similar in vitro profile to **1a**. While the *p*-alkoxy derivatives **11b**−**g** showed similar binding potencies, only the compounds bearing basic side-chains presented significantly higher cellular potency. In particular, the dimethylamine **11d** and the pyrrolidine **11e** gave a 37-fold and 10-fold increase, respectively, compared to compound **1a**. In contrast, the morpholino and imidazolyl derivatives **11f** and **11g**, while presenting binding affinity comparable to **11d** and **11e**, exhibited significantly lower cellular potency. Linking of basic side chains to the aryl ring via a methylene spacer showed that the length of the side chains had no impact on the binding affinity, with **12a** and **12b** being equipotent to their alkoxy analogues **11e** and **11f**. As was observed with the alkoxy derivatives, the basicity of the amino side chain appears to correlate with cellular potency, the pyrrolidine **12a** and the tetrahydro-2*H*-pyran-4-ylamine **12c** presenting 3-fold higher cellular potency than the morpholine **12b**. Replacement of the methylene linkage with a carbonyl group led to a decrease of the binding affinity for the pyrrolidine **13b** (5-fold versus **12a**) and the morpholine **13c** (3-fold versus **12b**). The nature of the amine (secondary versus primary) had also a significant impact on binding affinity. Indeed, replacement of morpholine **13c** with tetrahydro-2*H*-pyran-4-ylamine **13d** led to approximately a 7-fold increase in binding potency. Incorporation of a more flexible side chain led to lower binding affinity (**13a** versus **13d**). The gain in binding potency observed for **13d** (6-fold versus **1a**) translated to a similar increase in cellular potency. N-Methylation of the 4-aminotetrahydropyran group (**13e**) led to a drop of the binding affinity (approximately 10-fold versus **13d**). The same effect was observed for the inverse amide **14a**. The decrease in binding affinity resulting from these two structural modifications might be rationalized on the basis of our ALK5 model. Docking studies suggested that the amide N−H of **13d** might be involved in a hydrogen bond to the backbone C═O of both Glu284 and His285 or Glu284 alone (Figure 4). In contrast, the *N*-methyl analogue **13e** cannot H-bond via its amide nitrogen and the methyl group forces the amide further out of plane with the phenyl, thereby lowering binding affinity.

Thus, a significant improvement in both the binding affinity and cellular potency was achievable by varying the nature of the para side chain of the aryl ring. Furthermore, the nature of the para side chains also had a significant impact on the

Table 3. Rat Pharmacokinetics Profiles of **1a** and **13d**

compd	intrinsic clearance [mL·min^{-1}·(g of liver)$^{-1}$]	oral bioavailability[a] (F, %)	CLp[b] (mL min^{-1} kg^{-1})	Vdss[c] (L kg^{-1})	elimination $T_{1/2}$[d] (h)
1a	3	13 (21−5)	51 (moderate)	0.7	0.4
13d	1	17	20 (low)	1.4	1.3

[a] Bioavailability was calculated from the ratio of dose-normalized area under the curve values (AUC), using $AUC_{(0-\infty)}$ for animals dosed iv and $AUC_{(0-t)}$ for animals dosed po (where t is the last time point with measurable test compound concentrations). [b] CLp = systemic plasma clearance. [c] Vdss = steady-state volume of distribution. [d] $T_{1/2}$ = plasma half-life.

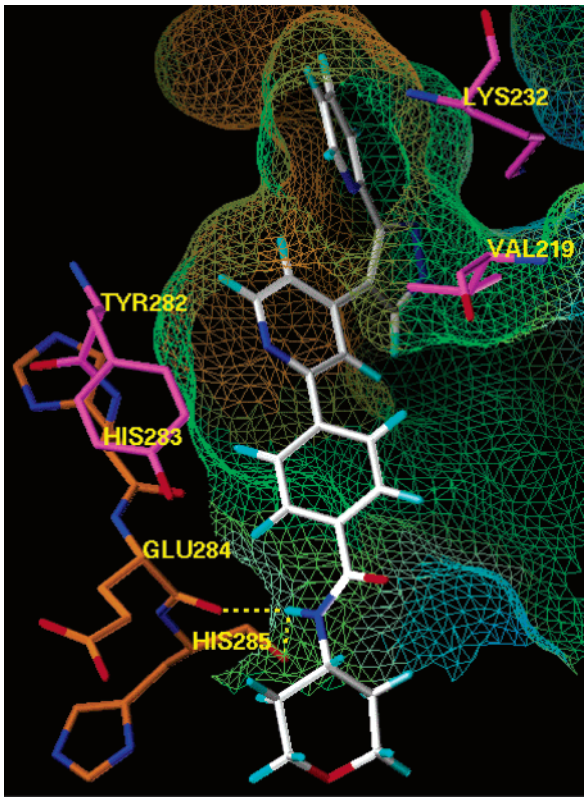

Figure 4. Binding mode hypothesis from docking study of **13d**.

pharmacokinetic profile of the compounds. Among the different compounds presenting cellular potency with IC_{50} < 100nM, **13d** exhibited an adequate pharmacokinetic profile in rats (plasma clearance less than 40 mL min^{-1}.kg^{-1} and half-life more than 2 h) to warrant further evaluation in vivo. **13d** was more stable in rat liver microsomes than the unsubstituted phenyl derivative **1a** (intrinsic clearance = 1 mL·min^{-1}·g^{-1} versus 3 mL·min^{-1}·g^{-1} for **1a**). Following iv and po administration to rats at doses of 2 and 4 mg/kg, respectively, a plasma clearance of 20 mL·min^{-1}·kg^{-1} was observed, equivalent to approximately 24% rat liver blood flow (cf. **1a**, 51 mL·min^{-1}·kg^{-1}). The lower plasma clearance of **13d** coupled with an increase in the volume of distribution resulted in a longer elimination half-life (1.3 h) compared with **1a** (0.4 h).

In Vivo Models and Results

To evaluate the in vivo efficacy of the phenylpyrazole derivatives **1a** and **13d**, the two compounds were tested in an acute model of dimethylnitrosamine- (DMN-) induced liver disease. [9] During fibrogenesis, increase in collagen IA1 synthesis is mainly triggered by TGF-β acting on hepatic stellate cells. DMN given for three consecutive days to rats increased collagen IA1 mRNA expression in the liver by about 10-fold at day 8. Compound **1a** (25−80 mg/kg b.i.d.) given on days 6, 7, and 8 by oral gavage to rats pretreated with DMN gave a dose-dependent inhibition of collagen IA1 overexpression (Figure 5). In this model, the two compounds produced qualitatively similar effects by inhibiting the DMN-induced collagen IA1 mRNA overexpression (Table 4). However their potencies differed as expected from their biological in vitro profile, compound **1a** being 6-fold less potent than compound **13d** in the cellular assay. Moreover, the greater activity of **13d** in vivo can also be attributed to a better pharmacokinetic profile than **1a** (Table 3).

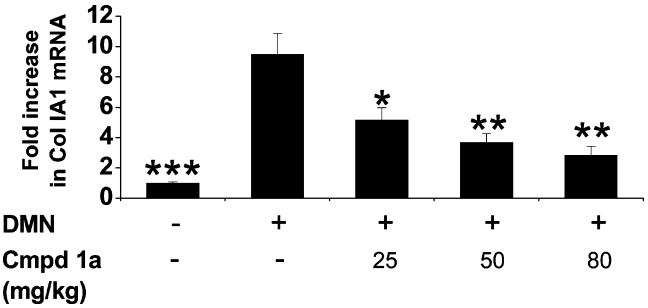

Figure 5. Dose−effect of compound **1a** administered orally (b.i.d.) in the acute rat DMN model (*p < 0.05 relative to DMN only; **p < 0.01;, ***p < 0.001, ANOVA).

Table 4. In Vivo Data[a] in the Acute DMN-Induced Liver Disease for Compounds **1a** and **13d**

compd	dose (mg·kg^{-1} po, b.i.d.)	collagen IA1 mRNA[b] (% inhibition)
1a	25	50.6 ± 9.6
13d	1	79.96 ± 1.4
13d	5	80.05 ± 2.7
13d	10	77.85 ± 1.05

[a] Experiments were performed with 5−8 animals/group. [b] Data are expressed as mean value ± SEM.

Effect of Compound 13d in an Acute Model of Renal Disease. To explore whether blocking ALK5 signaling would prevent TGF-β-induced expression of collagen IA1 in a renal model as well as in the liver model, compound **13d** was evaluated in a rat model of chemically induced renal fibrosis [11] at doses of 3 and 10 mg/kg u.i.d. Ten days after intraperitoneal injection of puromycin aminonucleoside (PAN), mRNA levels of collagen IA1 were increased (Figure 6). Relative collagen IA1 mRNA was significantly increased in total kidney by PAN from 1.0 ± 0.1 to 3.6 ± 0.2 (arbitrary units corrected by the rpL32 housekeeping gene, mean ± SEM of control and PAN−treated, respectively), and compound **13d** significantly decreased relative collagen IA1 mRNA levels at 3 and 10 mg/kg u.i.d. (2.4 ± 0.3 and 2.2 ± 0.3, respectively).

Selectivity Profile. Compound **13d** was tested against a panel of more than 10 kinases[12] (Table 5). Although excellent selectivity was obtained against most of these kinases, significant inhibition of p38α was observed at 10 μM. Compound binding to p38α was tested on purified recombinant GST-p38α, and the mean IC_{50} was 7.28 μM with 95% CL of 5.73−9.25 μM.

Conclusion

The aim of this work was to demonstrate that ALK5 inhibitors could inhibit, in vivo, the expression of collagen IA1, one key

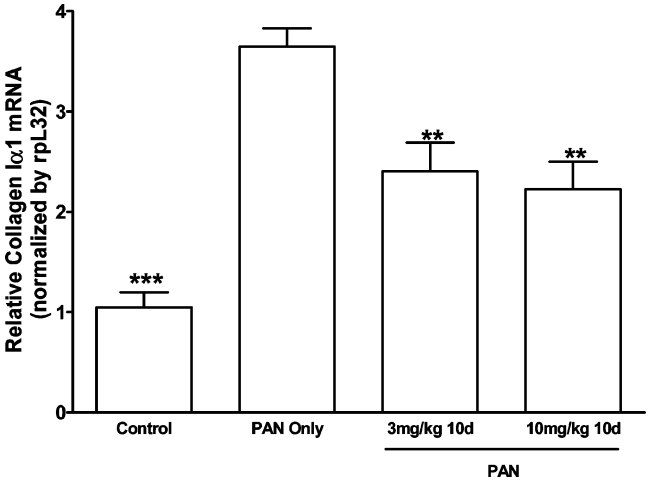

Figure 6. Effect of compound **13d** administered orally (u.i.d.) in acute rat PAN model for 10 days (**$p < 0.01$ relative to PAN only; ***$p < 0.001$, ANOVA).

Table 5. Selectivity of Compound **13d** against a Panel of Kinases

kinase	% inhibition[a]	kinase	% inhibition[a]
AMPK	15	P70S6K	−2
Chk1	5	PDK1	−10
CSK	19	PhosK	−27
JNK1	−1	PKA	−5
LCK	53	PKC A	6
MKK1	−3	SGK	5
MSK1	4	P38α	73
MAPK2	2	P38β	26

[a] Values are percent inhibition at 10 μM with 100 μM ATP. For kinases used and assay details, see ref 12.

component of the extracellular matrix, by blocking the TGF-β signaling pathway. Optimization of the phenylpyridine pyrazole series led to the identification of a potent and selective ALK5 inhibitor **13d** (GW788388). Indeed, substitution at the para position of the phenyl ring with a polar side chain not only improved the cellular potency (ca. 6-fold versus **1a**) but also decreased the in vivo plasma clearance in rats. Compound **13d** showed oral activity in models of liver and renal fibrosis. Compared to the unsubstituted compound **1a**, the *N*-(tetrahydro-2*H*-pyran-4-yl)carboxamide **13d** exhibited a significant improvement in oral activity with approximately 80% inhibition of collagen IA1 mRNA when tested at 1 mg/kg b.i.d. in the model of DMN-induced liver disease. Compound **13d** also presented activity in a PAN-induced model of kidney fibrosis by inhibiting collagen IA1 mRNA at doses of 3 and 10 mg/kg u.i.d. Although the overall impact of long-term blockade of ALK5 signaling is currently unknown and should be cautiously explored, the observation that potent ALK5 inhibitors can act both in vitro and in vivo to prevent overexpression of collagen IA1, a major extracellular matrix component in fibrotic diseases, suggests that ALK5 inhibition may represent a novel therapeutic approach to the treatment of fibrosis.

Experimental Section

All starting materials were commercially available and used without further purification. All reactions were carried out with the use of standard techniques under an inert atmosphere (Ar or N_2). Organic extracts were routinely dried over anhydrous sodium sulfate. Solvent removal refers to rotary evaporation under reduced pressure at 30−40 °C. Analytical thin-layer chromatography (TLC) was carried out on E. Merck 60-F_{254} precoated silica gel plates and components were usually visualized with UV light, iodine vapor, or Dragendorff preparation. Flash column chromatography was performed on silica gel, Merck grade 60 (230−400 mesh). Melting points were determined on a hot-stage Kofler apparatus and are uncorrected. Proton NMR (^{1}H NMR) spectra were recorded at ambient temperature on Bruker Avance 300 DPX spectrometers with tetramethylsilane as internal standard, and proton chemical shifts are expressed in parts per million (ppm) in the indicated solvent. The following abbreviations are used for multiplicity of NMR signals: s = singlet, d = doublet, t = triplet, q = quadruplet, dd = double doublet, m = multiplet, ddd = doublet of doublet of doublet, br s = broad singlet. Analytical HPLC (method A) was conducted on an X-Terra MS C18 column (2.5 μm, 30 × 3 mm i.d.) eluted with 0.01 M ammonium acetate in water (solvent A) and 100% acetonitrile (solvent B), according to the following elution gradient: 0−4 min, 0−100% B; 4−5 min, 100% B at a flow rate of 1.1 mL/min. Mass spectra (MS) were recorded on a micromass Platform-LC mass spectrometer in atmospheric pressure chemical positive ionization [AP + ve to give MH^+ molecular ions] or atmospheric pressure chemical negative ionization [AP − ve to give $(M - H)^-$ molecular ions] modes. Analytical HPLC (method B) was conducted on a Uptisphere-hsc column (3 μm, 33 × 3 mm i.d.) eluted with 0.01 M ammonium acetate in water (solvent A) and 100% acetonitrile (solvent B), according to the following elution gradient: 0−0.5 min, 5% B; 0.5−3.75 min, 5−100% B; 3.75−4.5 min, 100% B; 4.5−5 min, 100−5% B; 5−5.5 min, 5% B at a flow rate of 1.3 mL/min. Mass spectra (MS) were recorded on a micromass LCT mass spectrometer in electrospray positive ionization [ES + ve to give MH^+ molecular ions] or electrospray negative ionization [ES − ve to give $(M - H)^-$ molecular ions] modes.

The purity of the compounds was determined on two analytic high-performance liquid chromatography (HPLC) systems by UV detection (100% purity in both methods was obtained for the examples described below).

The intermediates 2-(2-fluorophenyl)-4-methylpyridine (**2b**), 2-(2-methylphenyl)-4-methylpyridine (**2c**), 2-(2-trifluorophenyl)-4-methylpyridine (**2d**), 2-(3-methylphenyl)-4-methylpyridine (**2e**), and 2-(3-methoxyphenyl)-4-methylpyridine (**2g**) were purchased from Avocado; 2-(3-trifluoromethylphenyl)-4-methylpyridine (**2f**) and 2-(4-methoxyphenyl)-4-methylpyridine (**2j**) were purchased from HFR.

General Procedure A: 2-Phenyl-4-(3-pyridin-2-yl-1*H*-pyrazol-4-yl)pyridine (1a). To a solution of intermediate **2a** (1 g, 3.64 mmol) in DMF (6 mL) at room temperature under N_2 was added dimethylformamide dimethylacetal (3 equiv, 1.5 mL). The mixture was stirred for 7 h at room temperature. Hydrazine monohydrate (excess, 6.9 mL) was added over 10 min, and then the mixture was warmed to 50 °C for 3 h and allowed to stand at room temperature overnight. The reaction mixture was quenched by addition of water (20 mL) and was extracted with CH_2Cl_2. The organic phases were combined, washed with brine, dried, and evaporated to dryness. The crude product was purified by column chromatography on silica gel eluted with CH_2Cl_2 and then with CH_2Cl_2/MeOH (98:2). Crystallization from a CH_2Cl_2/pentane mixture gave the title compound as an off-white powder (300 mg, 28%): mp 147 °C; ^{1}H NMR (300 MHz, $CDCl_3$) δ 8.64 (d, J = 5.1 Hz, 1H), 8.63 (br d, J = 4.9 Hz, 1H), 7.90 (dd, J = 7.9 and 1.3 Hz, 2H), 7.75 (s, 1H), 7.72 (s, 1H), 7.57 (ddd, J = 7.7, 7.5, and 1.3 Hz, 1H), 7.45−7.30 (m, 4H), 7.27−7.20 (m, 2H), NH (pyrazole not observed); MS (API) MH^+ 299; HR-MS calcd for $C_{19}H_{14}N_4$ (M + H) 299.1297, found 299.1252; analytical HPLC t_R = 2.56 min (A), t_R = 2.29 min (B).

2-[2-Fluorophenyl]-4-(3-pyridin-2-yl-1*H*-pyrazol-4-yl)pyridine (1b). Compound **1b** was prepared in 7% yield from **3b**: ^{1}H NMR (300 MHz, $CDCl_3$) δ 8.65 (d, J = 5.1 Hz, 1H), 8.63 (d, J = 4.9 Hz, 1H), 7.89 (ddd, J = 7.9, 7.7, and 1.9 Hz, 1H), 7.76 (s, 1H), 7.71 (s, 1H), 7.58 (ddd, J = 7.9, 7.5, and 1.7 Hz, 1H), 7.49 (d, J = 7.9 Hz, 1H), 7.35−7.12 (m, 4H), 7.05 (ddd, J = 8.1, 8.1, and 1.1 Hz, 1H), NH (pyrazole) not observed; MS (API) 317 (MH^+); HR-MS calcd for $C_{19}H_{13}FN_4$ (M + H) 317.1202, found 317.1187; analytical HPLC t_R = 2.49 min (A), t_R = 2.28 min (B).

2-(2-Methylphenyl)-4-[3-(pyridin-2-yl)-1*H*-pyrazol-4-yl]pyridine (1c). Compound **1c** was prepared from **2c** following method

A in 6.8% yield , after recrystallization from EtOAc: mp 149−151 °C; ^{1}H NMR (300 MHz, $CDCl_3$) δ 8.63 (d, J = 5.1 Hz, 1H), 8.59 (d, J = 4.5 Hz, 1H), 7.67 (s, 1H), 7.59 (ddd, J = 7.9, 7.7, and 1.7 Hz, 1H), 7.46 (d, J = 7.9 Hz, 1H), 7.39 (br s, 1H), 7.35−7.30 (m, 1H), 7.26 (dd, J = 5.1 and 1.7 Hz, 1H), 7.24−7.17 (m, 4H), 2.30 (s, 3H), NH (pyrazole) not observed; MS (API) *m*/*z* 313 (M + H)$^+$; HR-MS calcd for $C_{20}H_{16}N_4$ (M + H) 313.1453, found 313.1479; analytical HPLC t_R =2.56 min, 100% pure (A), t_R = 2.35 min, 100% pure (B).

2-[2-(Trifluoromethyl)phenyl]-4-(3-pyridin-2-yl-1*H*-pyrazol-4-yl)pyridine (1d). Compound **1d** was prepared in 12.4% yield, after recrystallization from EtOAc, from **2d** according to general method A: mp 173−175 °C, ^{1}H NMR (300 MHz, $CDCl_3$) δ 8.70 (d, J = 5.1 Hz, 1H), 8.67 (br d, J = 4 Hz, 1H), 7.79−7.73 (m, 2H), 7.70−7.58 (m, 2H), 7.56−7.44 (m, 4H), 7.40 (dd, J = 5.1 and 1.7 Hz, 1H), 7.32−7.26 (m, 1H), NH (pyrazole) not observed; MS (API) 367(M + H)$^+$; HR-MS calcd for $C_{20}H_{13}F_3N_4$ (M + H) 367.1170, found 367.1152; analytical HPLC t_R = 2.66 min (A), t_R = 2.42 min (B).

2-[3-Methylphenyl]-4-(3-pyridin-2-yl-1*H*-pyrazol-4-yl)pyridine (1e). Compound **1e** was prepared in 11% yield, after recrystallization from EtOAc, from **2e** according to general method A: mp 133−135 °C; ^{1}H NMR (300 MHz, $CDCl_3$) δ 8.57 (d, J = 4.7 Hz, 1H), 8.46 (d, J = 4.9 Hz, 1H), 7.92 (d, J = 7.9 Hz, 1H), 7.70 (ddd, J = 7.7, 7.5, and 1.7 Hz, 1H), 7.65 (br s, 1H), 7.57 (br d, J = 7.9 Hz, 1H), 7.54 (br s, 1H), 7.35 (ddd, J = 7.5, 7.5, and 1.1 Hz, 1H), 7.18 (dd, J = 7.7 and 7.8 Hz, 1H), 7.09−7.03 (m, 3H), 2.26 (s, 3H), NH (pyrazole) not observed; MS (API) 313 (M + H)$^+$; HR-MS calcd for $C_{20}H_{16}N_4$ 313.1453 (M + H), found 313.1448; analytical HPLC t_R = 2.73 min (A), t_R = 2.50 min (B).

2-[3-(Trifluoromethyl)phenyl]-4-(3-pyridin-2-yl-1*H*-pyrazol-4-yl)pyridine (1f). Compound **1f** was prepared in 14% yield from **2f** according to general method A: ^{1}H NMR (300 MHz, $CDCl_3$) δ 8.36 (d, J = 5 Hz, 2H), 8.12 (d, J = 8.9 Hz, 2H), 7.95 (s, 1H), 7.71(ddd, J = 7.7, 7.7, and 1.9 Hz, 1H), 7.67−7.52 (m, 3H), 7.22 (br d, J = 5.1 Hz, 2H), NH (pyrazole) not observed; MS (API) 367 (M + H)$^+$; HR-MS calcd for $C_{20}H_{13}F_3N_4$ 367.1170 (M + H), found 367.1128; analytical HPLC t_R = 3.01 min, (A), t_R = 2.73 min (B).

2-[3-Methoxyphenyl]-4-(3-pyridin-2-yl-1*H*-pyrazol-4-yl)pyridine (1g). Compound **1g** was prepared in 12% yield, after recrystallization from EtOAc, from **2g** according to general method A: mp 143−145 °C; ^{1}H NMR (300 MHz, $CDCl_3$) δ 8.87−8.83 (m, 2H), 7.96 (br s, 1H), 7.95 (s, 1H), 7.80 (ddd, J = 7.9, 7.7, and 1.7 Hz, 1H), 7.72 (br s, 1H), 7.66 (br d, J = 7.4 Hz, 2H), 7.56−7.39 (m, 3H), 7.13 (dd, J = 8 and 2.6 Hz, 1H), 4.40 (s, 3H), NH (pyrazole) not observed; MS (API) 329(M + H)$^+$; HR-MS : calcd for $C_{20}H_{16}N_4O$ 329.1402 (M + H), found 329.1395; analytical HPLC t_R = 2.58 min (A), t_R = 2.36 min (B).

2-[4-Methylphenyl]-4-(3-pyridin-2-yl-1*H*-pyrazol-4-yl pyridine (1h). Compound **1h** was prepared in 40% yield from **2h** according to general method A: ^{1}H NMR (300 MHz, $CDCl_3$) δ 8.62 (br d, J = 4.9 Hz, 2H), 7.80 (br d, J = 8.3 Hz, 2H), 7.72 (br s, 2H), 7.57 (ddd, J = 7.9, 7.9, and 1.7 Hz, 1H), 7.43 (br d, J = 7.9 Hz, 1H), 7.25−7.20 (m, 4H), 2.34 (s, 3H), NH (pyrazole) not observed; NH (pyrazole) not observed; MS (ES) 313 (M + H)$^+$; HR-MS calcd for $C_{20}H_{16}N_4$ 313.1453 (M + H), found 313.1404; analytical HPLC t_R = 2.43 min (A), t_R = 2.48 min (B).

2-[4-(Trifluoromethyl)phenyl]-4-(3-pyridin-2-yl-1*H*-pyrazol-4-yl)pyridine (1i). Compound **1i** was prepared in 27% yield, after recrystallization from ^{i}Pr2O/^{i}PrOH, from **2i** according to general method A: mp 155 °C; ^{1}H NMR (300 MHz, $CDCl_3$) δ 8.68 (d, J = 5 Hz, 1H), 8.63 (br d, J = 4.9 Hz, 1H), 8.02 (d, J = 8 Hz, 2H), 7.79 (br s, 1H), 7.74 (s, 1H), 7.67 (d, J = 8 Hz, 2H), 7.60 (ddd, J = 7.7, 7.7, and 1.7 Hz, 1H), 7.43 (d, J = 8 Hz, 1H), 7.31 (dd, J = 5.1 and 1.5 Hz, 1H), 7.24 (ddd, J = 4.9, 4.9, and 1.7 Hz, 1H), NH (pyrazole) not observed; MS (API) 367(M + H)$^+$; HR-MS calcd for $C_{20}H_{13}F_3N_4$ (M + H) 367.1170, found 367.1183; analytical HPLC t_R = 3.03 min (A), t_R = 2.76 min (B).

2-[4-Methoxyphenyl]-4-(3-pyridin-2-yl-1*H*-pyrazol-4-yl)pyridine (1j). Compound **1j** was prepared in 25% yield from **2j** according to general method A: ^{1}H NMR (300 MHz, $CDCl_3$) δ 8.84 (d, J = 5 Hz, 2H), 8.10 (d, J = 8.9 Hz, 2H), 7.94 (s, 1H), 7.92 (s, 1H), 7.80 (ddd, J = 7.7, 7.7, and 1.9 Hz, 1H), 7.66 (br d, J = 7.9 Hz, 1H), 7.47−7.40 (m, 2H), 7.17 (d, J = 8.9 Hz, 2H), 4.04 (s, 3H), NH (pyrazole) not observed; MS (API) 329 (M + H)$^+$; HR-MS calcd for $C_{20}H_{16}N_4O$ 329.1402 (M + H), found 329.1392; analytical HPLC t_R = 2.57 min (A), t_R = 2.35 min (B).

2-[4-Fluorophenyl]-4-(3-pyridin-2-yl-1*H*-pyrazol-4-yl)pyridine (1k). Compound **1k** was prepared in 17% yield, after recrystallization from ^{i}PrOH, from **2k** according to general method A: mp 117 °C; ^{1}H NMR (300 MHz, $CDCl_3$) δ 8.62 (br d, J = 4.9 Hz, 1H), 8.59 (d, J = 5.5 Hz, 1H), 7.91−7.82 (m, 2H), 7.71 (s, 1H), 7.68 (br s, 1H), 7.57 (ddd, J = 7.8, 7.8, and 1.7 Hz, 1H), 7.42 (d, J = 7.5 Hz, 1H), 7.25−7.16 (m, 2H), 7.06 (dd, J = 8.6 Hz, 2H), NH (pyrazole) not observed; MS (API) 317 (M + H)$^+$; HR-MS calcd for $C_{19}H_{13}FN_4$ (M + H) 317.1202, found 317.1210; analytical HPLC t_R = 2.66 min (A), t_R = 2.44 min (B).

2-[4-Isopropylphenyl]-4-[3-(pyridin-2-yl)-1*H*-pyrazol-4-yl]pyridine (1l). Compound **1l** was prepared in 16.5% yield from **2l** according to general method A: ^{1}H NMR (300 MHz, $CDCl_3$) δ 8.63 (br d, J = 4.9 Hz, 2H), 7.84 (d, J = 8.3 Hz, 2H), 7.74 (s, 1H), 7.72 (s, 1H), 7.58 (ddd, J = 7.7, 7.7, and 1.5 Hz, 1H), 7.43 (d, J = 7.9 Hz, 1H), 7.27 (d, J = 8.3 Hz, 2H), 7.22 (dd, J = 5.3 and 1.5 Hz, 1H), 7.19 (s, 1H), 2.99−2.81 (m, 1H), 1.21 (d, J = 6.7 Hz, 6H), NH (pyrazole) not observed; MS (ES) 341 (M + H)$^+$; HR-MS calcd for $C_{22}H_{20}N_4$ (M + H) 341.1766, found 341.1790; analytical HPLC t_R = 3.09 min (A), t_R = 2.84 min (B).

2-[4-Chlorophenyl]-4-(3-pyridin-2-yl-1*H*-pyrazol-4-yl)pyridine (1m). Compound **1m** was prepared in 5% from **2m** according to general method A: ^{1}H NMR (300 MHz, $CDCl_3$) δ 8.54−8.46 (m, 2H), 7.70 (d, J = 8.5 Hz, 2H), 7.58 (br s, 1H), 7.56 (br s, 1H), 7.44 (dd, J = 7.4 and 7.4 Hz, 1H), 7.28 (d, J = 7.5 Hz, 1H), 7.22 (d, J = 8.5 Hz, 2H), 7.14−7.04 (m, 2H), NH (pyrazole) not observed; MS (API) 333 (M + H)$^+$; HR-MS calcd for $C_{19}H_{13}ClN_4$ 333.0907 (M + H), found 333.0906; analytical HPLC t_R = 2.87 min (A), t_R = 2.65 min (B).

General Method B: 2-(4-Hydroxyphenyl)-4-(3-pyridin-2-yl-1-trityl-1*H*-pyrazol-4-yl)pyridine (7). A solution of **6** (4.6 g, 8.47 mmol) in toluene (100 mL) was treated with tetrakis(triphenylphosphine)palladium (0.83 g) and stirred at room temperature for 30 min. An aqueous solution of Na_2CO_3 (2 M, 22.58 mL) was added to the reaction mixture, followed by 4-hydroxyphenylboronic acid, pinacol ester (2.67equiv, 4.9 g, 22.31 mmol) in EtOH (30 mL). The resulting mixture was heated under reflux for 2 h. The cooled mixture was poured into ice and extracted with toluene. The organic layer was washed with water, dried over Na_2SO_4, and filtered. Evaporation of the solvent in vacuo gave a crude oil, which was purified by chromatography on silica gel (CH_2Cl_2/MeOH 98:2) to give **7** as a white solid (4.3 g, 91%), which contains the 2-trityl isomer as a minor component: mp 175°C; ^{1}H NMR (300 MHz, $CDCl_3$) δ 8.38 (d, J = 4.7 Hz, 1H), 8.31 (d, J = 5.5 Hz, 1H), 7.61−7.43 (m, 5H), 7.23−7.15 (m, 7H), 7.14−7.08 (m, 8H); 7.05−7.00 (m, 3H), 6.94 (dd, J = 5.3 and 1.5 Hz,1H), 6.59 (br d, J = 8.3 Hz, 2H); MS (API) 557 (M + H)$^+$.

4-[4-(3-Pyridin-2-yl-1-trityl-1*H*-pyrazol-4-yl)pyridin-2-yl]benzaldehyde (8). Compound **8** was prepared in 85% yield from **6** and 4-formylphenylboronic acid as described in general method B: ^{1}H NMR (300 MHz, $CDCl_3$) δ 10.08 (s, 1H), 8.61 (d, J = 5 Hz, 1H), 8.56 (d, J = 4 Hz, 1H), 8.18 (d, J = 8 Hz, 2H), 7.97 (d, J = 8 Hz, 2H), 7.95 (br s, 1H), 7.82 (d, J = 7.6 Hz, 1H), 7.74 (ddd, J = 7.6, 7.6, and 1.5 Hz, 1H), 7.66 (s, 1H), 7.42−7.34 (m, 8H), 7.33−7.23 (m, 10H); MS (API) 569 (M + H)$^+$.

4-[4-(3-Pyridin-2-yl-1-trityl-*1H*-pyrazol-4-yl)pyridin-2-yl]benzoic Acid Methyl Ester (9). Compound **9** was prepared in 83.6% yield from **6** and 4-(methoxycarbonylphenyl)boronic acid as described in general method B: ^{1}H NMR (300 MHz, $CDCl_3$) δ 8.50 (d, J = 5.1 Hz, 1H), 8.46 (d, J = 4.9 Hz, 1H), 8.02 (d, J = 8.5 Hz, 2H), 7.89 (d, J = 8.5 Hz, 2H), 7.80 (br s, 1H), 7.70 (d, J = 7.7 Hz, 1H), 7.63 (ddd, J = 7.9, 7.4, and 1.7 Hz, 1H), 7.56 (s, 1H), 7.32−7.25 (m, 7H), 7.05−7.00 (m, 10H), 3.86 (s, 3H); MS (API) 599 (M + H)$^+$.

4-[4-(3-Pyridin-2-yl-*1H*-pyrazol-4-yl)pyridin-2-yl]benzoic Acid Methyl Ester (1n). Compound **9** (0.1 g, 0.167 mmol) was treated with trifluoroacetic acid/CH_2Cl_2 (20/80, 10 mL) at room temperature overnight. The reaction mixture was neutralized with 1 N NaOH and extracted with CH_2Cl_2. The organic phase was dried over Na_2SO_4 and the solvent was evaporated in vacuo to give a crude oil, which was filtered on silica gel and precipitated with CH_2Cl_2/hexane to afford **1n** as a white solid (0.05 g, 84%): ^{1}H NMR (300 MHz, $CDCl_3$) δ 8.67 (d, J = 5.1 Hz, 1H), 8.61 (d, J = 4.3 Hz, 1H), 8.08 (d, J = 8.5 Hz, 2H), 7.98 (d, J = 8.5 Hz, 2H), 7.80 (br s, 1H), 7.73 (br s, 1H), 7.58 (ddd, J = 7.9, 7.7, and 1.5 Hz, 1H), 7.42 (d, J = 7.7 Hz, 1H), 7.32 (d, J = 4.9 and 1.3 Hz, 1H), 7.26−7.21 (m, 1H), 4.00 (s, 3H), NH (pyrazole) not observed; MS (API) 357(M + H)$^+$; HR-MS calcd for $C_{21}H_{16}N_4O_2$ (M + H) 357.1351, found 357.1377; analytical HPLC t_R = 2.64 min (A), t_R = 2.42 min (B).

2-[4-Cyanophenyl]-4-(3-pyridin-2-yl-1H-pyrazol-4-yl)pyridine (1o). Compound **1o** was prepared in 93% yield from **6** and 4-cyanophenylboronic acid as described in general method B: ^{1}H NMR (300 MHz, $CDCl_3$) δ 8.53 (br d, J = 5.1 Hz, 2H), 7.90 (d, J = 8.5 Hz, 2H), 7.65 (s, 1H), 7.61 (s, 1H), 7.56 (d, J = 8.5 Hz, 2H), 7.47 (dd, J = 7.7 and 7.5 Hz, 1H), 7.30 (d, J = 6.8 Hz, 1H), 7.18 (d, J = 4.5 Hz, 1H), 7.11 (br s, 1H), NH (pyrazole) not observed; MS (API) 324 (M + H)$^+$; HR-MS calcd for $C_{20}H_{13}N_5$ 324.1249 (M + H), found 324.1279; analytical HPLC t_R = 2.51 min (A), t_R = 2.34 min (B).

O-Alkylation General Procedure: 2-{4-[(2-Cyclohexylethyl)-oxy]phenyl}-4-[3-(pyridin-2-yl)-1*H*-pyrazol-4-yl]pyridine (11a). To a solution of **7** (0.091 g, 0.17 mmol) in DMF (2 mL) were added potassium carbonate (4 equiv, 0.09 g, 0.65 mmol) and (2-bromoethyl)cyclohexane (1.3 equiv, 0.04 g, 0.21 mmol). The reaction mixture was then heated to 50 °C overnight and the resulting suspension was filtered after cooling. The filtrate was concentrated, dissolved in ethyl acetate, and washed with brine. The organic layer was dried over Na_2SO_4, filtered, and evaporated to give the trityl compound as an oil. This compound was deprotected without purification. The crude material was dissolved in methanol (10 mL)/HCl 1 N (3 mL). The solution was heated under reflux overnight. The reaction mixture was concentrated in vacuo, and the residue was dissolved in water and washed with CH_2Cl_2. The aqueous layer was basified with NaOH 1 N and extracted with EtOAc. The organic extract was washed with water and dried over Na_2SO_4, filtered, and evaporated to give a solid, which was purified by chromatography on silica gel (CH_2Cl_2/MeOH 9:1) to give **11a** as a white solid (0.035 g, 48%): ^{1}H NMR (300 MHz, $CDCl_3$) δ 8.60 (d, J = 5.1 Hz, 2H), 7.86 (d, J = 8.9 Hz, 2H), 7.72 (s, 1H), 7.61−7.56 (m, 1H), 7.46 (br s, 1H), 7.22−7.19 (m, 3H), 6.91 (d, J = 8.9 Hz, 2H), 3.98 (t, J = 6.6 Hz, 2H), 1.72−1.60 (m, 6H), 1.51−1.39 (m, 1H), 1.26−1.08 (m, 4H), 0.96−0.85 (m, 2H), NH (pyrazole) not observed; MS (API) 425 (M + H)$^+$; HR-MS calcd for $C_{27}H_{28}N_4O$ 425.2341 (M H), found 425.2336; analytical HPLC t_R = 3.82 min (A), t_R = 3.04 min (B).

2-{4-[(2-Chloroethyl)oxy]phenyl}-4-[3-(pyridin-2-yl)-1*H*-pyrazol-4-yl]pyridine (11b). Compound **11b** was prepared in 28% yield from **7** and 1,2-dichoroethane as described for compound **11a**: ^{1}H NMR (300 MHz, $CDCl_3$) δ 8.61 (m, 2H), 7.89 (d, J = 8.7 Hz, 2H), 7.74 (br s, 2H), 7.50 (t, J = 7.7 Hz, 1H), 7.45 (d, J = 7.5 Hz, 1H), 7.24 (d, J = 4.9 Hz, 2H), 6.95 (d, J = 8.7 Hz, 2H), 4.23 (t, J = 6 Hz, 2H), 3.78 (t, J = 6 Hz, 2H), NH (pyrazole) not observed; MS (API) 377 (M + H)$^+$; HR-MS calcd for $C_{21}H_{17}ClN_4O$ 377.1169 (M + H), found 377.1141; analytical HPLC t_R = 2.78 min (A), t_R = 2.52 min (B).

1-[(4-{4-[3-(Pyridin-2-yl)-1*H*-pyrazol-4-yl]-pyridin-2-yl}phenyl)-oxy]-2-propanone (11c). Compound **11c** was prepared from **7** and 1,2-dichoroethane as described for **11a**: ^{1}H NMR (300 MHz, $CDCl_3$) δ 8.63 (d, J = 4.5 Hz, 1H), 8.59 (d, J = 5.1 Hz, 1H), 7.87 (d, J = 8.9 Hz, 2H), 7.72 (s, 1H), 7.68 (s, 1H), 7.58 (ddd, J = 7.9, 7.5, and 1.7 Hz, 1H), 7.43 (d, J = 8 Hz, 1H), 7.25−7.16 (m, 2H), 6.90 (d, J = 9 Hz, 2H),4.53 (s, 2H), 2.23 (s, 3H), NH (pyrazole) not observed; MS (API) 371 (M + H)$^+$; HR-MS calcd for $C_{22}H_{18}N_4O_2$ 371.1508 (M + H), found 371.1520; analytical HPLC t_R = 2.39 min (A), t_R = 2.17 min (B).

Dimethyl-{2-[(4-{4-[3-(pyridin-2-yl)-1*H*-pyrazol-4-yl]-2-pyridinyl}phenyl)oxy]ethyl}amine (11d). Compound **11d** was prepared in 39% yield from **7** and 2-chloro-*N*,*N*-dimethylethylamine as described for **11a**: ^{1}H NMR (300 MHz, $CDCl_3$) δ 8.83−8.77 (m, 2H), 8.04 (d, J = 9 Hz, 2H), 7.90 (s, 1H), 7.88 (s, 1H), 7.76 (ddd, J = 7.9, 7.7, and 1.7 Hz, 1H), 7.61 (br d, J = 7.9 Hz, 1H), 7.44−7.34 (m, 2H), 7.14 (d, J = 9 Hz, 2H), 4.27 (t, J = 5.7 Hz, 2H), 2.92 (t, J = 5.7 Hz, 2H), 2.51 (s, 6H), NH (pyrazole) not observed; MS (API) 386 (M + H)$^+$; HR-MS calcd for $C_{23}H_{23}N_5O$ 386.1981 (M + H), found 386.1978; analytical HPLC t_R = 2.11 min (A), t_R = 2.09 min (B).

2-[4-(2-{1*H*-Imidazol-1-yl}-ethoxy)phenyl]-4-(3-pyridin-2-yl-1*H*-pyrazol-4-yl)pyridine (11g). Compound **11g** was prepared in 16% yield from **7** and *N*-(2-chloroethyl)imidazole hydrochloride as described for compound **11a**: ^{1}H NMR (300 MHz, $CDCl_3$) δ 8.63−8.55 (m, 2H), 7.86 (d, J = 8.9 Hz, 2H), 7.70 (s, 1H), 7.67 (s, 1H), 7.65 (s, 1H), 7.55 (ddd, J = 7.9, 7.7, and 1.7 Hz, 1H), 7.42 (d, J = 8.1 Hz, 1H), 7.24−7.15 (m, 2H), 7.02 (d, J = 9 Hz, 2H), 6.88 (d, J = 8.9 Hz, 2H), 4.35−4.27 (m, 2H), 4.25−4.17 (m, 2H), NH (pyrazole) not observed; MS (API) 409 (M + H)$^+$; HR-MS calcd for $C_{24}H_{20}N_6O$ 409.1777 (M + H), found 409.1779; analytical HPLC t_R = 2.34 min (A), t_R = 2.09 min (B).

2-[4-(2-Pyrrolidin-1-ylethoxy)phenyl]-4-(3-pyridin-2-yl-1*H*-pyrazol-4-yl)pyridine (11e). Compound **11e** was prepared as a white solid in 23% yield from **7** and *N*-(2-chloroethyl)pyrrolidine hydrochloride as described for **11a**: mp 135 °C; ^{1}H NMR (300 MHz, $CDCl_3$) δ 8.63−8.53 (m, 2H), 7.85 (d, J = 8.9 Hz, 2H), 7.70 (s, 1H), 7.68 (s, 1H), 7.56 (dd, J = 7.9 and 7.5 Hz, 1H), 7.42 (d, J = 7.9 Hz, 1H), 7.24−7.15 (m, 2H), 6.93 (d, J = 8.9 Hz, 2H), 4.17 (t, J = 5.5 Hz, 2H), 2.97 (t, J = 5.3 Hz, 2H), 2.72 (br s, 4H), 1.82 (br s, 4H), NH (pyrazole) not observed; MS (API) 412 (M + H)$^+$; HR-MS calcd for $C_{25}H_{25}N_5O$ 412.2137 (M + H), found 412.2137; analytical HPLC t_R = 2.17 min (A), t_R = 2.26 min (B).

4-{2-[(4-{4-[3-(Pyridin-2-yl)-1*H*-pyrazol-4-yl]-pyridin-2-yl}-phenyl)oxy]ethyl}morpholine (11f). Compound **11f** was prepared in 29.2% yield from **7** and *N*-(2-chloroethyl)morpholine hydrochloride as described for **11a**: mp 138 °C; ^{1}H NMR (300 MHz, $CDCl_3$) δ 8.58 (d, J = 4.9 Hz, 2H), 7.83 (d, J = 8.9 Hz, 2H), 7.69 (s, 1H), 7.65 (br s, 1H), 7.54 (ddd, J = 7.9, 7.7, and 1.7 Hz, 1H), 7.39 (d, J = 7.9 Hz, 1H), 7.18−7.11 (m, 2H), 6.9 (d, J = 8.9 Hz, 2H), 4.11 (t, J = 5.6 Hz, 2H), 3.69 (t, J = 4.7 Hz, 4H), 2.80 (t, J = 5.7 Hz, 2H), 2.62 (t, J = 4.5 Hz, 4H), NH (pyrazole) not observed; MS (API) 429 (M + H)$^+$; HR-MS calcd for $C_{25}H_{25}N_5O_2$ 428.2086 (M + H), found 428.2069; analytical HPLC t_R = 2.42 min (A), t_R = 2.13 min (B).

4-Aminotetrahydropyran. To a solution of tetrahydropyran-4-one (13.12 mL, 0.142mol) in ethanol were added hydroxylamine hydrochloride (41.5 g, 0.597mol) and sodium acetate (40.82 g, 0.497mol). The mixture was heated at reflux for 20 h. The precipitate was filtered and the filtrate was evaporated. The product was crystallized from tBuOMe (26 g, 100%). This product (16.33 g, 0.142 mol) was dissolved in anhydrous THF under nitrogen atmosphere, and $LiAlH_4$ (640 mL, 0.639 mol) was added dropwise at 0 °C. The reaction mixture was stirred at room temperature for 2 days and heated to reflux for 6 h. The reaction mixture was then treated with an aqueous solution of NaOH (10%, 260 mL) at 0 °C. The precipitate was filtered and the filtrate was evaporated to give a yellow oil (11.9 g, 83%): ^{1}H NMR (300 MHz, $CDCl_3$) δ 3.69 (d, J = 12.1 Hz, 2H), 3.12 (td, J = 11.6 and 2 Hz, 2H), 2.63−2.55 (m, 1H), 1.50 (dd, J = 12.6 and 2 Hz, 2H), 1.13 (td, J = 3 and 11.6 Hz, 2H).

[(4-{4-[3-(Pyridin-2-yl)-1*H*-pyrazol-4-yl]-pyridin-2-yl}phenyl)-methyl]tetrahydro-2*H*-pyran-4-ylamine (12c). To a solution of **8** (64.69 g, 0.114mol) and 4-aminotetrahydropyran (11.5 g, 0.114mol) in CH_2Cl_2 (750 mL) were added, at room temperature under nitrogen, AcOH (0.1 equiv, 6.5 mL) and $NaHB(OAc)_3$ (2 equiv, 48.22 g, 0.227 mol). The mixture was stirred at room temperature overnight. The reaction mixture was neutralized with a saturated aqueous solution of $NaHCO_3$ (1 L) at 20 °C and stirred for 15 min. The mixture was extracted with CH_2Cl_2 (2 × 500 mL). The organic phase was washed with water (500 mL), dried over

Na_2SO_4, filtered, and evaporated in vacuo. The crude material was dissolved in MeOH/HCl (3:2, 1.3 L). The solution was heated to reflux for 2.5 h. The reaction mixture was concentrated in vacuo. The residue was dissolved in water (250 mL) and washed with CH_2Cl_2 (2 × 250 mL). The aqueous layer was basified with NaOH 1 N (530 mL) and extracted with CH_2Cl_2 (3 × 250 mL). The organic phase was washed with water (250 mL), dried over Na_2SO_4, filtered, and evaporated to give a crude product, which was purified by chromatography on silica gel and eluted with CH_2Cl_2/MeOH (95:5 and 80:20) to give **12c** as a white solid (13.67 g, 29%): mp 79 °C; ^{1}H NMR (300 MHz, $CDCl_3$) δ 8.61 (d, J = 5.1 Hz, 2H), 7.86 (d, J = 8.1 Hz, 2H), 7.72 (s, 1H), 7.70 (s, 1H), 7.56 (ddd, J = 7.6, 8, and 1.5 Hz, 1H), 7.42 (d, J = 8.1 Hz, 1H), 7.36 (d, J = 8.1 Hz, 2H), 7.21 (d, J = 5 Hz, 2H), 3.91 (br d, J = 11.1 Hz, 2H), 3.83 (s, 2H), 3.31 (ddd, J = 11.6, 11.7, and 1.5 Hz, 2H), 2.73−2.66 (m, 1H), 1.81 (br d, J = 14.1, 2H), 1.42 (q, J = 12.2 Hz, 2H), NH (pyrazole) not observed; MS (API) 412 (M + H)$^+$; HR-MS calcd for $C_{25}H_{25}N_5O$ 412.2137 (M + H), found 412.2108; analytical HPLC t_R = 2.09 min (A), t_R = 1.94 min (B).

4-[3-(Pyridin-2-yl)-1*H*-pyrazol-4-yl]-2-[4-(1-pyrrolidinylmethyl)phenyl]pyridine (12a). Compound **12a** was prepared from **8** and pyrrolidine following the method described for **12c** to give a white solid (25%): ^{1}H NMR (300 MHz, $CDCl_3$) δ 8.71 (d, J = 5.1 Hz, 1H), 8.69 (br d, J = 4.9 Hz, 1H), 7.97 (d, J = 8.3 Hz, 2H), 7.82 (br s, 1H), 7.79 (s, 1H), 7.66 (ddd, J = 7.8, 7.8, and 1.7 Hz, 1H), 7.55 (d, J = 8.1 Hz, 2H), 7.50 (d, J = 7.9 Hz, 1H), 7.32−7.31 (m, 2H), 3.87 (s, 2H), 2.84−2.71 (m, 4H), 1.95−1.90 (m, 4H), NH (pyrazole) not observed; MS (API) 382 (M + H)$^+$; HR-MS calcd for $C_{24}H_{23}N_5$ 382.2032 (M + H), found 382.2040; analytical HPLC t_R = 2.07 min (A), t_R = 2.06 min (B).

4-[(4-{4-[3-(Pyridin-2-yl)-1*H*-pyrazol-4-yl]-2-pyridinyl}phenyl)-methyl]morpholine Hydrochloride (12b). Compound **12b** was prepared from **9** and morpholine following the method described for **12c** to give white crystals (14.4%): mp 248°C; ^{1}H NMR (300 MHz, DMSO-d_6) δ 8.78−8.63 (m, 3H), 8.48 (s, 1H), 8. 8.25−8.08 (m, 3H), 8.01−7.83 (m, 4H), 7.64 (m, 1H), 4.46 (br s, 2H), 4.03−3.80 (m, 4H), 3.30−3.03 (m, 4H), NH (pyrazole) not observed; MS (API) 398 (M + H)$^+$; HR-MS calcd for $C_{24}H_{23}N_5O$·HCl 398.1981 (M + H), found 398.1967; analytical HPLC t_R = 2.39 min (A), t_R = 2.18 min (B).

***N*-[2-(Methoxy)ethyl]-4-{4-[3-(pyridin-2-yl)-1*H*-pyrazol-4-yl]-pyridin-2-yl}benzamide (13a).** To a solution of 2-methoxyethylamine (0.053 g, 0.7 mmol), HOAt (0.095 g, 0.7 mmol), and DCC (110 μL, 0.7 mmol) in DMF (15 mL) was added **9** (1 equiv, 0.4 g, 1 mmol). The reaction mixture was stirred overnight at room temperature. The mixture was evaporated to dryness, treated with a mixture of MeOH/HCl 1 N (3:2, 10 mL), and then heated to reflux overnight. The reaction mixture was concentrated in vacuo, and the residue was dissolved in water and washed with CH_2Cl_2. The aqueous phase was basified with NaOH 1 N and extracted with CH_2Cl_2. The organic extract was washed with water, dried over Na_2SO_4, filtered, and evaporated to give a product, which was purified by chromatography on silica gel and eluted with CH_2Cl_2/CH_3OH (95:5) to give a colorless oil **13a** (0.104 g, 37%): mp 95 °C; ^{1}H NMR (300 MHz, $CDCl_3$) δ 8.63 (d, J = 5.1 Hz, 1H), 8.57 (d, J = 4.7 Hz, 1H), 7.95 (d, J = 8.3 Hz, 2H), 7.79 (d, J = 8.3 Hz, 2H), 7.75 (s, 1H), 7.69 (s, 1H), 7.54 (ddd, J = 7.5, 7.5, and 1.5 Hz, 1H), 7.38 (d, J = 7.9 Hz, 1H), 7.25 (dd, J = 5.1 and 1.6 Hz, 1H), 6.85−6.75 (m, 1H), 3.62−3.45 (m, 4H), 3.31 (s, 3H), NH (pyrazole) not observed; MS (API) 400 (M + H)$^+$; HR-MS calcd for $C_{23}H_{21}N_5O_2$ 400.1773 (M + H), found 400.1777; analytical HPLC t_R = 2.19 min (A), t_R = 1.98 min (B).

2-Pyrrolidin-1-yl-*N*-{4-[4-(3-pyridin-2-yl-1*H*-pyrazol-4-yl)-pyridin-2-yl]phenyl}acetamide (13b). Compound **13b** was prepared in 71% yield from **9** and pyrrolidine following the method described for **13a**: mp 118 °C; ^{1}H NMR (300 MHz, $CDCl_3$) δ 8.66 (d, J = 5.1 Hz, 1H), 8.58 (m, 1H), 7.95 (d, J = 8.3 Hz, 2H), 7.76 (br s, 1H), 7.57 (d, J = 8.3 Hz, 2H), 7.38−7.35 (m, 2H), 7.25−7.18 (m, 2H), 3.59 (t, J = 6.9 Hz, 2H), 3.38 (t, J = 6.6 Hz, 2H), 1.93−1.80 (m, 4H), NH (pyrazole) not observed; MS (API) 396 (M + H)$^+$; HR-MS calcd for $C_{24}H_{21}N_5O$ 396.1824 (M + H), found 396.1816; analytical HPLC t_R = 2.34 min (A), t_R = 2.13 min (B).

2-Morpholin-1-yl-*N*-{4-[4-(3-pyridin-2-yl-1*H*-pyrazol-4-yl)-pyridin-2-yl]phenyl}acetamide (13c). Compound **13c** was prepared in 73% yield from **9** and morpholine as described for compound **13a**: mp 155 °C; ^{1}H NMR (300 MHz, $CDCl_3$) δ 13.2 (br s, 1H), 8.74−8.46 (m, 2H), 8.30 (br s, 1H), 8.16−7.98 (m, 3H), 7.94−7.77 (m, 2H), 7.52 (d, J = 8.1 Hz, 2H), 7.45−7.29 (m, 2H), 3.71−3.60 (m, 4H), 3.58−3.40 (m, 4H); MS (API) 412 (M + H)$^+$; HR-MS calcd for $C_{24}H_{21}N_5O_2$ 412.1773 (M + H), found 412.1777; analytical HPLC t_R = 2.20 min (A), t_R = 1.98 min (B).

4-{4-[3-(Pyridin-2-yl)-1*H*-pyrazol-4-yl]-pyridin-2-yl}-*N*-(tetrahydro-2*H*-pyran-4-yl)benzamide (13d). Compound **13d** was prepared in 36% yield from **9** and 4-aminotetrahydropyran following the method described for **13a**: mp 254 °C; ^{1}H NMR (300 MHz, $CDCl_3$) δ 8.58 (m, 2H), 8.40 (d, J = 7.6 Hz, 2H), 8.09 (m, 3H), 7.95 (d, J = 8.1 Hz, 2H), 7.89 (d, J = 7.2 Hz, 1H), 7.41−7.37 (m, 2H), 4.04−4.02 (m, 1H), 3.89 (d, J = 9.4 Hz, 2H), 3.37 (d, J = 11.1 Hz, 2H), 1.77 (d, J = 11.1 Hz, 2H), 1.65−1.58 (m, 2H), NH (pyrazole) not observed; MS (API) 426 (M + H)$^+$; HR-MS calcd for $C_{25}H_{23}N_5O_2$ 426.1930 (M + H), found 426.1921; analytical HPLC t_R = 2.22 min (A), t_R = 2 min (B).

***N*-Methyl-4-{4-[3-(pyridin-2-yl)-1*H*-pyrazol-4-yl]-pyridin-2-yl}-*N*-(tetrahydro-2*H*-pyran-4-yl)benzamide (13e).** Compound **13e** was prepared from in 41% yield from **9** and *N*-methyltetrahydro-2*H*-pyran-4-amine [13] as described for **13a**: mp 104 °C; ^{1}H NMR (300 MHz, $CDCl_3$) δ 8.47 (br s, 1H), 8.42 (d, J = 4.9 Hz, 1H), 7.93−7.91 (m, 3H), 7.73 (ddd, J = 7.7, 7.9, and 1.5 Hz, 1H), 7.31 (d, J = 8.3 Hz, 2H), 7.26−7.24 (m, 3H), 4.08−4.01 (m, 2H), 3.51−3.40 (m, 2H), 2.68−2.58 (m, 1H), 2.50 (s, 3H), 1.95−1.85 (m, 2H), 1.50−1.37 (m, 2H), NH (pyrazole) not observed; MS (API) 440 (M + H)$^+$; HR-MS calcd for $C_{26}H_{25}N_5O_2$ 440.2086 (M + H), found 440.2081; analytical HPLC t_R = 2.29 min (A), t_R = 2.04 min (B).

***N*-(4-{4-[3-(Pyridin-2-yl)-1*H*-pyrazol-4-yl]-pyridin-2-yl}phenyl)-tetrahydro-2*H*-pyran-4-carboxamide (14a).** Compound **6** (0.844 g, 1.5 mmol) was coupled with 4-aminophenylboronic acid, pinacol ester (0.396 g, 1.8 mmol) as described in general method B to afford (4-{4-[3-(2-pyridinyl)-1-trityl-1*H*-pyrazol-4-yl]-2-pyridinyl}phenyl)-amine (**10**) as a white solid (0.45 g).This material was used in the next step without further purification. MS(ES) 556 (M + H)$^+$. Compound **14a** was prepared in 12% yield from **10** and tetrahydropyran-4-ylcarboxylic acid following the method described for **13a**: ^{1}H NMR (300 MHz, $CDCl_3$) δ 8.60 (d, J = 5 Hz, 2H), 7.87 (d, J = 8.6 Hz, 2H), 7.71 (s, 1H), 7.59−7.54 (m, 3H), 7.42 (d, J = 8 Hz, 1H), 7.32 (s, 1H), 7.23−7.19 (m, 2H), 4.04−3.96 (m, 2H), 3.44−3.35 (m, 2H), 2.51−2.40 (m, 1H), 1.90−1.77 (m, 4H), NH (pyrazole) not observed; MS (API) 426 (M + H)$^+$; HR-MS calcd for $C_{25}H_{23}N_5O_2$ 426.1930 (M + H), found 426.1914; analytical HPLC t_R = 2.28 min (A), t_R = 2.07 min (B).

Molecular Modeling. The docking experiments were performed with GOLD V1.1 [14] in TGF-β−FKBP12 complex. A single hydrogen-bond constraint was added during calculations, guiding the 4-pyridine N1 to interact with the protein backbone NH of His-283. Parameters were maintained as standard default GOLD V1.1 settings with the following exceptions. The floodfill radius, defining the active-site search center, was increased to 12 Å. This radius was measured from a dummy atom located at the centroid generated from the heavy atom positions of five key residues: Lys-232, Leu-260, Ser-280, His-283, and Asp-351. Ten poses per ligand docking were saved, and the top-scoring pose was taken to be the favored pose in the majority of cases. Only in the event of an obvious failure was the top pose discarded and an alternative, lower-scoring pose selected. To ensure that a range of solutions was available for scrutiny, early termination was disabled. Visualization was performed with Sybyl 6.x (Tripos) and Insight II (Accelrys).

ALK5 Fluorescence Polarization Binding Assay. Compound binding to ALK5 was tested on purified recombinant GST−ALK5 (residues 198−503). Displacement of rhodamine green fluorescently labeled ATP competitive inhibitor[15] by different concentrations of test compounds was used to calculate a binding pIC_{50}. GST−ALK5

was added to a buffer containing 62.5 mM *N*-(2-hydroxyethyl)-piperazine-*N*′-2-ethanesulfonic acid (Hepes), pH 7.5, 1 mM dithiothreitol (DTT), 12.5 mM $MgCl_2$, 1.25 mM 3-[(3-cholamidopropyl)-dimethylammonio]-1-propanesulfonic acid (CHAPS) (all reagents obtained from Sigma), and 1 nM rhodamine green-labeled ligand so that the final ALK5 concentration is 10 nM based on active-site titration of the enzyme. The enzyme/ligand reagent (40 μL) was added to 384-well assay plates containing 1 μL of different concentrations of test compound. The plates are read immediately on a LJL Acquest fluorescence reader (Molecular Devices) with excitation, emission, and dichroic filters of 485, 530, and 505 nm, respectively. The fluorescence polarization for each well is calculated by the Acquest and is then imported into curve-fitting software for construction of concentration−response curves.

Cellular Assays To Measure Anti-TGF-β Activity of ALK5 Inhibitors. Activity of compounds was tested in a transcriptional assay in HepG2 cells. Cells were stably transfected with a PAI-1 promoter driving a luciferase (firefly) reporter gene.[16] The stably transfected cells responded to TGF-β stimulation by a 10−20-fold increase in luciferase activity compared to control conditions.

To test anti-TGF-β activity of compounds, cells were seeded in 96-well microplates at a concentration of 35 000 cells/well in 200 μL of serum-containing medium. Microplates were then placed for 24 h in a cell incubator at 37 °C in a 5% CO_2 atmosphere. Compound dissolved in dimethyl sulfoxide (DMSO) was then added at concentrations of 50 nM−10 μM (final concentration of DMSO 1%) for 30 min prior to addition of recombinant TGF-β (1 ng/mL) (R&D Systems). After an overnight incubation, cells were washed with phosphate-buffered saline (PBS) and lysed by addition of 10 μL of passive lysis buffer (Promega). Inhibition of luciferase activity relative to control groups was used as a measure of compound activity. A concentration−response curve was constructed, from which an IC_{50} value was determined graphically.

p38α Fluorescence Polarization assay. Compound **13d** binding to p38α was tested on purified recombinant GST-p38α. Displacement of a rhodamine green fluorescently labeled ATP competitive inhibitor by different concentrations of test compounds was used to calculate a binding IC_{50}. GST−p38α was added to a buffer containing 62.5 mM Hepes, pH 7.4, 1 mM DTT, 12.5 mM $MgCl_2$, 1.25 mM CHAPS (all reagents obtained from Sigma), and 1.25−5 nM rhodamine green-labeled ligand, so that the final p38α concentration was 5−50 nM. The enzyme/ligand reagent (30 μL) was added to 384-well assay plates containing 1 μL of different concentrations of test compound. The plates were incubated for 45 min and then read on a LJL Acquest fluorescence reader (Molecular Devices) with excitation, emission, and dichroic filters of 485, 530, and 505 nm, respectively. The fluorescence polarization for each well was calculated by the Acquest and was then imported into curve-fitting software for construction of concentration−response curves.

Animal Models. All experimental protocols were performed in accordance with the policies of the Institutional Animal Care and Use Committee. Animals were fed with a standard diet and had free access to water.

Acute DMN Model. Male Sprague-Dawley rats weighing 200−225 g were treated for three consecutive days (days 1−3) with 12.5 mg/kg ip DMN (dimethylnitrosamine, Sigma) or saline. Animals were then treated orally (po) b.i.d. with compound or its vehicle [20% HCl 1 N, 80% HPMC (0.5%), and Tween 80 (5%), adjusted to pH 4] in a volume of 4 mL/kg on days 6, 7, and 8. Animals were sacrificed on day 8, 2 h after the fifth administration of compound or vehicle. Livers were collected for collagen IA1 mRNA quantification by RT-PCR. Results are reported as percent inhibition of DMN-induced increase in collagen IA1 compared to control. Collagen IA1 mRNA was quantified relative to ribosomal 18S. Four to six rats were used in each group.

Messenger RNAs were quantified by RT-PCR on an ABI prism 7700 sequence detection system (Applied Biosystem). All genes were quantified relative to 18S (Taqman ribosomal RNA control reagent, Applied Biosystems). Primer sequences for Collagen IA1 (COL IA1) are as follows: ATGTTCAGCTTTGTGGACCT (forward) and CAGCTGACTTCAGGGATGT (reverse).

After collection, livers were kept at −20 °C in RNAlater. RNAs were then extracted by use of the RNAble kit (Eurobio, France). Reverse transcription of 1 μg of total RNA was carried out with the Taqman reverse transcription reagent (Applied Biosystem). PCR was performed with the sybr-green technology in a final volume of 25 μL. Briefly, 5 μL of cDNA was mixed with 12.5 μL of sybr-green master mix and 0.1 μL of each primer (50 pmol/μL); after a 10 min incubation at 95 °C, amplification was achieved by 40 cycles of 15 s at 95 °C followed by 1 min at 65 °C. On each amplification curve, the threshold cycle was determined and used for quantification of mRNA by use of the ABI prism 7700 software.

Acute PAN Model. Sprague-Dawley (SD) rats (250−308 g) were used in this study. Animals where housed individually in metabolism cages. Compound **13d** and vehicle were given by oral gavage once a day (u.i.d.). To induce renal disease, SD rats were injected intraperitonally with 15 mg/100 g puromycin aminonucleoside (PAN) (Sigma, St. Louis, MO) in 0.9% saline.

SD rats were pretreated by oral gavage with vehicle (20 rats), 3 mg/kg (10 rats), or 10 mg/kg (10 rats) of compound **13d** u.i.d.. To determine the effect of compound **13d** on renal disease, PAN was injected at 15 mg/100 g to 10 vehicle-treated animals and all rats receiving **13d** on the next day. Saline (0.9%) was injected intraperitoneally in the remaining 10 vehicle (control) rats. At day 10, after the PAN injection, the animals were terminated by carbon dioxide asphyxiation. Kidneys were collected for analysis. At termination, kidneys were harvested and immediately snap-frozen in liquid nitrogen. Guanidinium thiocyanate (GTC; 4 M, 5 mL) was added to 300 mg of kidney tissue. The kidneys were homogenized in the GTC with a motorized homogenizer. The homogenate was layered over 4.5 mL of 5.7 M cesium chloride in ultracentrifuge tubes. The tubes were centrifuged at 50 000 rpm for 24 h at 20 °C. The cesium gradient was withdrawn, leaving behind the RNA in a pellet. The pellet was cleaned in ethanol and resuspended in diethyl pyrocarbonate-treated water. RNA quantity was determined by optical density at 260 nm. RNA (20 μg) was treated with DNase for 15 min at 37 °C. The DNase was deactivated at 70 °C for 10 min.

cDNA was synthesized from 20 μg of the DNase-treated RNA with reverse transcriptase and buffer provided by Applied Biosystems. Synthesis was performed in 96-well plates in the 6700 Nucleic Acid Workstation (Applied Biosystems, Foster City, CA) according to the manufacturer's instructions. mRNA levels were detected by quantitative reverse transcriptase polymerase chain reaction (RT-PCR) by use of the Taqman system by Applied Biosystems. The robotic workstation was also used to set up quantitative RT-PCR plates, adding the probes and primers to the cDNA, along with Taqman universal PCR master mix (Applied Biosystems). To each well was added 20 μL of master mix containing 100 nM target probe, 200 nM forward target primer, and 200 nM reverse target primer. Quantification of collagen IA1 mRNA was expressed as arbitrary units corrected by the rpL32 housekeeping gene. For rat collagen IA1, the target probe was 6FAM-TTGCATAGCTCGC-CATCGCACA-TAMRA, the forward primer was TATGCT-TGATCTGTATCTGCCACAAT, and the reverse primer was TCGCCCTCCCGTTTTTG. For rat RPL-32, the target probe was 6FAM-CGCAAAGCCATCGTGGAAAGAGCT-TAMRA, the forward primer was CGCTCACAATGTTTCCTCCA, and the reverse primer was TGACTCTGATGGCCAGTTGG.

Statistical analysis was performed on the data with GraphPad PRISM software (San Diego, CA). Statistical significance was determined by one-way analysis of variation (ANOVA) followed by Bonferroni post hoc test. Group data are reported as mean ± SEM.

Metabolic Incubations. Incubation mixtures consisted of liver microsomes (0.5 mg of microsomal protein/mL), substrates (3.0 μM), $MgCl_2$ (5 mM), and nicotinamide adenine dinucleotide phosphate, reduced form (NADPH; 0.48 mM) in a total volume of 1.5 mL Tris buffer (0.1 M, pH 7.4). Incubations were open to the air at 37 °C. At $T = 0$ and at three time points ranging up to 30 min, aliquots (200 μL) were removed and precipitated with the same

volume of acetonitrile. The whole sample was vortexed and centrifuged. For the analysis, 50 μL of supernatant was injected into the chromatographic system. The compound was analyzed by an HPLC method with a spectrophotometric detection. Separation was made on a C18 column (50 × 4.6 mm, 4 μm; Phenomenex Luna). The flow rate was 2 mL/min and the mobile phase composition was 50 mM CH_3COONH_4/acetonitrile (gradient, 5 min).

Determination of the in Vitro $T_{1/2}$. The analyte peak area was converted to percentage drug remaining, with the $T = 0$ peak area value taken as 100%. The slope of the linear regression from log percentage remaining versus incubation time relationships ($-k$) was used in the conversion to in vitro Cl_{int} (in units of milliliters per minute per gram) according to $Cl_{int} = (0.693/\text{in vitro } T_{1/2})(45/0.5)$, where 45 mg g^{-1} was the value used for the concentration of liver microsomal proteins.

Rat Pharmacokinetic Study. Compounds were administered singly as solutions, either intravenously (iv) as a bolus or orally (po) via gavage to male Sprague-Dawley rats (Charles River, U.K.) weighing between 220 and 260 g, at nominal doses of 2 mg/kg iv and 4 mg/kg po. Two rats were dosed per route. Animals were housed in standard holding cages with water and food available ad libitum. All doses were prepared in vehicle containing 12.5% DMSO, 2.5% 1 M HCl, 20% PEG200, and 65% sodium acetate (0.09 M) (final pH > 3.5) excepting the oral dose for **13d**, which was formulated in 4% DMSO and 96% [0.5% HPMC/5% Tween/20%HCl (1 M) in NaH_2PO_4 (0.1 M)], and **1a**, which was prepared in 10% DMSO and 90% water adjusted to pH 4 with acetic acid. Serial blood samples (0.35 mL) were collected from each animal via a lateral tail vein into heparin microtainers at various time points for 6 h post-ose.

The final time points from each animal were terminal, obtained after anaesthesia with isofluorane and exsanguination. Plasma was prepared from blood samples by centrifugation and stored frozen prior to analysis. Compounds were extracted from plasma by precipitation with three parts acetonitrile to one part plasma. Extracted samples were centrifuged and the supernatant was dried under nitrogen gas at 40 °C and then reconstituted in the LC mobile phase. Plasma concentrations of test compounds were determined by liquid chromatography−tandem mass spectrometry (LC-MS/MS) with multiple reaction monitoring in positive turbo ion spray ionization mode on a Perkin-Elmer Sciex API365 mass spectrometer. Compounds were separated on a C18 Phenomenex Luna column (5 cm × 2 mm, 5 μm) by reverse-phase chromatography.

Pharmacokinetic parameters were calculated by noncompartmental analysis with an in-house Excel-based macro. The iv half-lives were determined by log linear regression analysis. Oral bioavailability was calculated from the ratio of dose normalized area under the curve values (AUC), with $AUC_{(0-\infty)}$ for animals dosed iv and $AUC_{(0-t)}$ for animals dosed po.

Acknowledgment. We gratefully acknowledge Gaël Krysa and Valérie Boullay for performing the cellular assays and running the in vivo rat model, Claudette Mookherjee for performing rat pharmacokinetic studies, and Ruolan Wang for running the Alk5 binding assay. A special thanks to Frédéric Donche and Géraldine Poulain for their contribution to the synthesis of the described compounds and to Mélanie Barnathan for her assistance in mass spectra. We also thank Andrew Brewster for valuable comments during the preparation of the manuscript.

Supporting Information Available: Structure of the fluorescent ligand for the FP assay; experimental procedures for intermediates **2a**−**k**, **3a**−**m**, and **4**−**6;** and LC/MS and HPLC data for final compounds. This material is available free of charge via the Internet at http://pubs.acs.org.

References

(1) (a) Massague, J.; Blain, S. A.; Lo, R. S. TGFβ Signaling in Growth Control, Cancer, and Heritable Disorders. *Cell* **2000**, *103*, 295−309. (b) Border, W. A.; Noble, N. A. Transforming growth factor β in tissue fibrosis. *N. Engl. J. Med.* **1994**, *331*, 1286−1292. (c) Blobe, G. C.; Schiemann, W. P.; Lodish, H. F. Role of transforming growth factor beta in human disease. *N. Engl. J. Med.* **2000**, *342*, 1350−1358.

(2) Derynck, R.; Zhang, Y.; Feng, X.-H. Transcriptional Activators of TGF-β Responses: Smads. *Cell* **1998**, *95*, 737−740.

(3) Schnabl, B.; Kweon, Y. O.; Frederick, J. P.; Wang, X. F.; Rippe, R. A.; Brenner, D. A. The role of Smad3 in mediating mouse hepatic stellate cell activation. *Hepatology* **2001**, *34*, 89−100.

(4) Nakamura, T.; Sakata, R.; Ueno, T.; Sata, M.; Ueno, H. Inhibition of transforming growth factor beta prevents progression of liver fibrosis and enhances hepatocyte regeneration in dimethylnitrosamine-treated rats. *Hepatology* **2000**, *32*, 247−255.

(5) Kopp, J. B.; Factor, V. M.; Mozes, M.; Nagy, P.; Sanderson, N.; Bottinger, E. P.; Klotman, P. E.; Thorgeirsson, S. S. Transgenic mice with increased plasma levels of TGF-β1 develop progressive renal disease. *Lab. Invest.* **1996**, *74*, 991−1003.

(6) (a) Border, W A.; Okuda, S.; Languino, L R.; Sporn, M B.; Ruoslahti, E. Suppression of experimental glomerulonephritis by antiserum against transforming growth factor beta 1. *Nature* **1990**, *346*, 371−374. (b) Sharma, K.; Jin, Y.; Guo, J. Ziyadeh, F. N. Neutralization of TGF-β by anti-TGF-β antibody attenuates kidney hypertrophy and the enhanced extracellular matrix gene expression in STZ-induced diabetic mice. *Diabetes* **1996**, *45*, 522−530. (c) Ziyadeh, F N.; Hoffman, B. B.; Han, D. C.; Iglesias-De La Cruz, M. C.; Hong, S. W.; Isono, M.; Chen, S.; McGowan, T A.; Sharma, K. Long-term prevention of renal insufficiency, excess matrix gene expression, and glomerular mesangial matrix expansion by treatment with monoclonal antitransforming growth factor-beta antibody in db/db diabetic mice. *Proc. Natl. Acad. Sci. U.S.A.* **2000**, *97*, 8015−8020.

(7) Gellibert, F.; Woolven, J.; Fouchet, M.-H.; Mathews, N.; Goodland, H.; Lovegrove, V.; Laroze, A.; Nguyen, V.-L.; Sautet, S.; Wang, R.; Janson, C.; Smith, W.; Krysa, G.; Boullay, V.; de Gouville, A.-C.; Huet, S.; Hartley, D. Identification of 1,5-Naphthyridine Derivatives as a Novel Series of Potent and Selective TGF-β Type I Receptor Inhibitors. *J. Med. Chem.* **2004**, *47*, 4494−4506.

(8) Sawyer, J. S.; Anderson, B. D.; Beight, D. W.; Campbell, R. M.; Jones, M. L.; Herron, D. K.; Lampe, J. W.; McCowan, J. R.; McMillen, W. T.; Mort, N.; Parsons, S.; Smith, E. C. R.; Vieth, M.; Weir, L. C.; Yan, L.; Zhang, F.; Yingling, J. M. Synthesis and Activity of New Aryl- and Heteroaryl-Substituted Pyrazole Inhibitors of the Transforming Growth Factor-β Type I Receptor Kinase Domain. *J. Med. Chem.* **2003**, *46*, 3953−3956.

(9) De Gouville, A. C.; Boullay, V.; Krysa, G.; Pilot, J.; Brusq, J. M.; Loriolle, F.; Gauthier, J. M.; Papworth, S. A.; Laroze, A.; Gellibert, F.; Huet, S. Inhibition of TGF-beta signaling by an ALK5 inhibitor protects rats from dimethylnitrosamine-induced liver fibrosis. *Br. J. Pharmacol.* **2005**, 1−12.

(10) Huse, M.; Chen, Y. G.; Massagué, J.; Kuriyan, J. Crystal structure of the cytoplasmic domain of the type I TGF β receptor in complex with FKBP12. *Cell* **1999**, *96*, 425−436.

(11) (a) Chandra, M.; Susin, M.; Teichberg, S.; McVicar, M. Experimental focal segmental glomerulosclerosis: correlation with protein excretion, glomerular filtration rate, and renal plasma flow. *Pediatr. Res.* **1984**, *18*, 1195−1201. (b) Van Goor, H.; Diamond, J. R.; Grond, J. Renal Disease Induced in Rats by Puromycin Aminonucleoside, in *Experimental and Genetic Rat Models of Chronic Renal Failure*; Gretz, N., Strauch, M., Eds.; Karger: Basel, Switzerland, 1993; pp 68−81. (c) Yamazaki, T. Podocytic degeneration and regeneration in puromycin aminonucleoside nephropathy in the rat. *Pathol. Int.* **1995**, *45*, 465−472.

(12) Dundee Panel. Davies, S. P.; Reddy, H.; Caivano, M.; Cohen, P. Specificity and mechanism of action of some commonly used protein kinase inhibitors. *Biochem. J.* **2000**, *351*, 95−105.

(13) Hashimoto, H.; Ikemoto, T.; Itoh, T.; Maruyama, H.; Hanaoka, T.; Wakimasu, M.; Mitsudera, H.; Tomimatsu, K. Process Development of 4-[*N*-Methyl-*N*-(tetrahydropyran-4-yl)aminomethyl]aniline Dihydrochloride: A Key Intermediate for TAK-779, a Small-Molecule Nonpeptide CCR5 Antagonist. *Org. Process Res. Dev.* **2002**, *6*, 70−73.

(14) Jones, G.; Willett, P.; Glen, R. C.; Leach, A. R.; Taylor, R. Development and Validation of a Genetic Algorithm for Flexible Docking. *J. Mol. Biol.* **1997**, *267*, 727−748.

(15) The fluorescent ligand is described in the following patent application: Patent WO02/24680, 2000.

(16) Dennler, S.; Itoh, S.; Vivien, D.; ten Dijke, P.; Huet, S.; Gauthier, J. M. Direct binding of Smad3 and Smad4 to critical TGF-B inducible elements in the promoter of human plasminogen activator inhibitor-type 1 gene. *EMBO J.* **1998**, *17*, 3091−3100.

JM0509905